

Fault-tolerant hierarchical energy management system for an electrical power system on more-electric aircraft

Xin Wang^{a,*}, Jason Atkin^b, Serhiy Bozhko^a

^a Power Electronics Machines and Control Research Group, Faculty of Engineering, University of Nottingham, Nottingham NG7 2RD, UK

^b Computational Optimisation and Learning Lab, School of Computer Science, University of Nottingham, Nottingham NG7 2RD, UK

HIGHLIGHTS

- Proposing a fault-tolerant hierarchical EMS for an aircraft EPS to ensure system resilience in multiple faulty scenarios;
- Proposing a MILP-MPC strategy to optimise the long-term performance of the system considering future predictions;
- Proposing deterministic rule-based control strategies to cope with system real-time changes with a fast clock;
- Proposing four modes for the low level of the EMS to either cooperate collaboratively or independently;
- Considering various normal and faulty conditions during the flight, including both EMS external and internal faults.

ARTICLE INFO

Keywords:

Energy management system
Model predictive control
Hierarchical control
Fault tolerant control
Electrical power system
More electric aircraft

ABSTRACT

The concept of More-Electric Aircraft (MEA) has the potential to improve the environmental, economic, and reliability performance in the energy and transportation sectors. To achieve this potential, it has become a tendency to develop complex architectures of Electrical Power Systems (EPSs) for MEA to supply increasing electrical power demands. Moreover, a reliable and intelligent Energy Management System (EMS) is critical to coordinate the various EPS subsystems to ensure safe and efficient flight, following the real-time EPS operating requirements and safety criteria, while reducing the operating costs for all flight stages. This paper presents a fault-tolerant hierarchical EMS, for an innovative multi-converter-based aircraft EPS, to configure the system, ensure power distribution, and manage energy storage in multiple faulty scenarios over different time scales. There are two levels in this EMS: The High Level (HL) is based on Model Predictive Control (MPC), formulated by Mixed-Integer-Linear-Programming (MILP), to optimise the long-term EPS performance while considering future predictions; The Low Level (LL) adopts deterministic rules to cope with load changes and fault occurrences over the short term, during the HL sample intervals, with a faster clock. In particular, the LL controller contains four modes: to either cooperate with the HL online MPC or to operate independently, in either EPS normal or faulty conditions. The proposed EMS is evaluated in two cases, firstly considering load deviations in a normal operating scenario, and then considering behaviour in fault scenarios. The results indicate that the proposed EMS successfully reduces the EPS operational costs while ensuring quick responses to dynamic changes with either EPS component faults or EMS internal faults.

1. Introduction and literature review

1.1. Background and motivation

In a little more than a century, commercial aviation has evolved into the fastest, safest, and most far-reaching transportation mode [1,2]. However, the aircraft sector has recently been more and more focused

on the resulting environmental challenges [3,4]. Many initiatives have been proposed to reduce the emissions in the next generation of aircraft currently being developed, such as Power Optimized Aircraft (POA), More Open Electrical Technologies (MOET) project [5], the CLEAN SKY Joint Undertaking (CSJU) and Clean Aviation Joint Undertaking [6], targeting international goals to reach net-zero emissions by 2050 [7–9]. As a result, the concept of More Electric Aircraft (MEA) has been proposed as a major development trend for future aircraft to improve

* Corresponding author.

E-mail address: xin.wang4@nottingham.ac.uk (X. Wang).

<https://doi.org/10.1016/j.apenergy.2024.124955>

Received 23 June 2024; Received in revised form 19 October 2024; Accepted 16 November 2024

Available online 29 November 2024

0306-2619/© 2024 The Authors. Published by Elsevier Ltd. This is an open access article under the CC BY-NC-ND license (<http://creativecommons.org/licenses/by-nc-nd/4.0/>).

Nomenclature

Indices of EPS architecture

j, l	Index for HV and LV buses respectively
c	Index for cells (modular DC/DC converters)
p, q	Index for HV and LV loads respectively
N^{APU}	Number of APU
N^{HVB}	Number of HV buses
N^{LVB}	Number of LV buses
N^C	Number of cells
N^{BAT}	Number of batteries
N^{HVLcri}, N^{HVLncr}	Number of HV critical/non-critical loads
N^{LVLcri}, N^{LVLncr}	Number of LV critical/non-critical loads

Indices of the EMS

H	Prediction horizon
k	Time intervals, $k \in \mathbb{Z}_{\geq 0}$
T_s	Sampling time
N	Total time steps
$\Gamma^{on}\{*\}$	The recommendation values from the online MPC to the low-level control
$\Gamma^{off}\{*\}$	The recommendation values from the offline dataset to the low-level control
$M\{*\}$	The measurement value from EPS to the EMS
T_s^{HL}, k^{HL}	Sample time/Time step of high-level control
T_s^{LL}, k^{LL}	Sample time/Time step of low-level control

Parameters of EPS

Power limitations

$PMAX^G$	Initial estimation of maximum generator and APU output power [kW]
P^{AHVmax}	Maximum output power of APU bus to HV buses [kW]
P_{jj}^{HVmax}	Maximum power of HV buses [kW]
P_{jc}^{HVCmax}	Maximum power of connection link between HV bus j and cell c [kW]
p^{Cmax}	Rated power of DC/DC converter cells [kW]
P_{cl}^{LVCmax}	Maximum power of connection link between cell c and LV bus j [kW]
$P_l^{dismax}, P_l^{chmax}$	Maximum charging and discharging power for each battery l [kW]
P_{ll}^{LVmax}	Maximum power of LV buses [kW]

ESS limitations

B_l^{cap}	Capacity of battery l [kWh]
HI, LO	Upper/Lower boundary for battery state of charge
Efficiency	
η_j^{AHV}	Transmission efficiency in cables between the APU bus and HV bus j
η_{jj}^{HV}	Transmission efficiency in cables of HV bus connection between bus j and j'
η_{jc}^{HVC}	Transmission efficiency in cables between the HV bus j and cell c
η_c	Efficiency of cell c
η_{cl}^{LVC}	Transmission efficiency in cables between the cell c and LV bus l
$\eta_l^{ch}, \eta_l^{dis}$	Charging/ Discharging efficiency of battery l
η_{ll}^{LV}	Transmission efficiency in cables of LV bus connection between bus l and l'

Load priority

λ_{jp}^{HVLncr}	The priority of the p th non-critical load on HV bus j
λ_{jq}^{LVLncr}	The priority of the q th non-critical load on LV bus l

Parameters of the EMS

Load power

$P_{jp}^{HVLcri}(k)$	The p th critical load power on HV bus j [kW]
$P_{jp}^{HVLncr}(k)$	The p th non-critical load power on HV bus j [kW]
$P_{lq}^{LVLcri}(k)$	The q th critical load power on LV bus l [kW]
$P_{lq}^{LVLncr}(k)$	The q th non-critical load power on LV bus l [kW]

Failure

$\gamma_j^G(k)$	Indicator for the failure of generator j
$\gamma_{jc}^{HVC}(k)$	Indicator for the failure of connection link between HV bus j and cell c
$\gamma_{cl}^{LVC}(k)$	Indicator for the failure of connection link between cell c and LV bus l
$\gamma^C(k)$	Indicator for the failure of cell c
$\gamma_l^{BAT}(k)$	Indicator for the failure of battery l
APU status $R^{APU}(k)$	Indicator for the starting status of APU: when $R^{APU}(k) = 0$, APU is not ready for connection, when $R^{APU}(k) = 1$, APU is ready for connection

Continuous decision variables of the EMS

Power

$P^{Gmax}(k)$	Maximum output power of generator/APU [kW]
$P^{APU}(k)$	Power flowing from APU to the APU bus [kW]
$P_j^{AHVp}(k)$	Power flowing from APU bus to the HV bus j [kW]
$P_j^{AHVn}(k)$	Power flowing from HV bus j to the APU bus [kW]
$P_j^G(k)$	Power flowing from generator j to corresponding HV bus j [kW]
$P_{jj}^{HV}(k)$	Power flowing from HV bus j to HV bus j' [kW]
$P_{jc}^{HVC}(k)$	Power flowing from HV bus j to cell c [kW]
$P_{cl}^{LVC}(k)$	Power flowing from cell c to LV bus l [kW]
$P_l^{ch}(k), P_l^{dis}(k)$	Charging/ Discharging power of battery on LV bus l [kW]
$P_{ll}^{LV}(k)$	Power flowing from LV bus l to LV bus l' [kW]
ESS	
$SOC_l(k)$	State of charge of battery on LV bus l
$\delta_l(k)$	Tolerance for upper bound of state of charge of battery on LV bus l
$\varepsilon_l(k)$	Tolerance for lower bound of state of charge of battery on LV bus l

Binary decision variables of the EMS

Connections

$S^{APU}(k)$	Connection status of the link between APU and APU bus
$S_j^{AHV}(k)$	Connection status of the link between APU bus and HV bus j
$S_j^G(k)$	Connection status of the link between generator j and corresponding HV bus j
$S_{jj}^{HV}(k)$	Connection status of the link between HV bus j and HV bus j'
$S_{jp}^{HVLncr}(k)$	Connection status of the p th non-critical load power on HV bus j
$S_{jc}^{HVC}(k)$	Connection status of the link between HV bus j and cell c
$S_{cl}^{LVC}(k)$	Connection status of the link between cell c and LV bus l
$S_l^{BAT}(k)$	Connection status of the link between LV bus l and its corresponding battery
$S_{ll}^{LV}(k)$	Connection status of the link between LV bus l and LV bus l'
$S_{lq}^{LVLncr}(k)$	Connection status of the q th non-critical load power on LV bus l

Indicators of Power direction

$s_j^{AHVp}(k)$	Indicator for power flow direction from APU bus to the HV
-----------------	---

	bus j		
$s_j^{AHVn}(k)$	Indicator for power flow direction from HV bus j to the APU bus	$s_l^{disch}(k)$	Indicator for discharging the battery on LV bus l
$s_{jj}^{HV}(k)$	Indicator for power flow direction HV bus j to HV bus j	$s_{ll}^{LV}(k)$	Indicator for power flow direction from LV bus l to LV bus l
$s_{jj}^{HV}(k)$	Indicator for power flow direction HV bus j to HV bus j	$s_{ll}^{LV}(k)$	Indicator for power flow direction from LV bus l to LV bus l
$s_l^{ch}(k)$	Indicator for charging the battery on LV bus l		APU starting decisions
		$ST^{APU}(k)$	Indicator for the starting of APU: when $ST^{APU}(k) = 0$, do not start APU, when $R^{APU}(k) = 1$, start APU

energy efficiency and reduce gas emissions [10]. In MEA, several subsystems that once relied on hydraulic, mechanical, or pneumatic power have been completely or partially replaced by electrical systems [11,12]. The electrification change increases the complexity of the aircraft Electric Power System (EPS), encouraging the development of novel architectures consisting of various power sources and Energy Storage Systems (ESSs), buses with different voltage levels, numerous power electronics converters with switches for flexible power transmission, as well as increasing electrical power demands [13–15].

To cope with the increasingly complex onboard EPS, a more reliable and intelligent Energy Management System (EMS) is required to configure the system (i.e., opening/closing of interconnection switches), to ensure power distribution, and to manage load demands and energy storage, following the real-time EPS operating requirements and safety criteria, while reducing the operating costs for all flight stages. Considering the EPS dynamics/changes at different time scales, the EMS must be able to control EPS operations over multiple time-scales, with both fast reactions to ensure safety in the short-time (e.g., reacting to changing power demands to avoid overloads or lack of power), and longer term planning to improve efficiency, reduce switching/load shedding/losses, and accommodate longer term safety issues such as ensuring that flight-critical loads can remain powered in any power shortage circumstances. Consequently, a hierarchical control architecture can reasonably be adopted in the EMS to handle these different time scales [16,17]. In addition, the design has to be resilient to faults in communication, and decisions must be deterministic and replicable. Consequently, designing a fault-tolerant hierarchical EMS is critical but complex.

1.2. Literature review

Various algorithms have previously been studied for EMSs for different EPSs. Aided by predefined safety and operational rules, the MEA EPS reconfiguration solutions are studied in [18,19], considering different failure scenarios and power loss minimisation, respectively. In [20,21], a deterministic rule-based EMS is proposed to provide power scheduling and emergency backup for a PV-battery-based and grid-integrated microgrid. In [22], the rules are compiled as a Finite State Machine (FSM) to realise the EPS reconfiguration operation in MEA. An FSM is also adopted in [23] to schedule power and energy storage for battery/supercapacitor/fuel cell hybrid source vehicles meeting dramatic changes in motor power demands. In addition, an improved FSM method is proposed in [24] to define states based on both the battery's SOC and the stored hydrogen level for a renewable energy microgrid. Although the authors of [21] argue that deterministic rule-based methods are considered reliable and resilient for real-time responses, optimisation-based methods are widely proposed for optimal control sequences for an EPS and have better adaptivity to new operational conditions. For example, [25] shows that the proposed Dynamic Programming (DP)-based optimal EMS reduces the equivalent energy consumption of the HEV by 6.1 % compared to the rule-based EMS, although the rule-based method has robustness and low computational loads. Moreover, [26] concludes that, compared to the FSM method, the proposed Genetic Algorithm (GA) and Simulated Annealing optimization Algorithm (SAA) achieve a 40 % and 19.3 % cost saving, respectively, when managing power scheduling of a hybrid energy system

integrating batteries and renewable energy sources.

As reviewed in [27–29], a variety of algorithms have been applied in energy management strategies, such as Dynamic Programming (DP), Mixed-Integer Linear Programming (MILP), and Mixed Integer Quadratic Programming (MIQP), GA, Particle Swarm Optimisation (PSO), Machine Learning (ML), etc. A DP-based EMS is proposed in [30] to reduce the hydrogen consumption and ageing costs of an ESS for an aircraft battery-fuel cell system. The study compares the EMS performance for five potential EPS configurations, indicating the advantage of fuel cell active configuration. Researchers in [31] present the formulation of a MILP-based EMS for large-scale power distribution networks, integrating renewable energy sources, considering bidirectional power flows and ESS degradation, aiming to reduce maintenance costs, power losses, and voltage fluctuations. MILP-based EMS is also studied in [32] to optimise the day-ahead energy scheduling and pricing strategies for a multi-energy microgrid considering uncertainties of renewable generation. In [33], an MIQP-based EMS is proposed for an MEA to optimise the power-sharing among generators and the ESS on one HV bus to improve the generator efficiency and the usage of the ESS. In [34,35], EMS strategies are proposed for aircraft to meet the targets of reducing block fuel burn, energy consumption, and emissions, as well as meeting flight missions. The proposed EMSs adopt Non-dominated Sorting Genetic Algorithm II (NSGA-II), addressing the design trade-off. PSO-based EMS is proposed for the aircraft electromechanical system in [36], to minimise the fuel consumption of the aircraft engine and maximise the cooling efficiency. [37,38] propose EMSs based on reinforcement learning algorithms for multi-stack fuel cell hybrid vehicles and hybrid electric propulsion aircraft, respectively. In [37], the proposed EMS maintains battery state of charge (SOC) and minimises hydrogen consumption with the consideration of fuel cell failure situations. The proposed EMS in [38] optimises the thrust distribution and power distribution to reduce aircraft fuel consumption. The aforementioned studies do not consider real-time EPS reconfiguration for power distribution, aiming for techno-economic benefits as presented in [22]. In [39], a GA-based algorithm is proposed to reconfigure PV arrays for stratospheric airships, in order to improve the output power with a smooth P–V curve.

In general, algorithms such as MILP and MIQP are categorized as classical optimisation, while other algorithms, such as GA and PSO, are categorized as soft computing [40]. Researchers compare the two categories of energy management studies in [40,41]. In [41], MILP and NSGA-II methods-based EMS are compared to optimise the operating cost and CO₂ emissions for the operation planning of a district energy system when considering uncertainties in energy demands and renewable energy generation. The study shows that MILP performs better than NSGA-II in several aspects, such as computation time, implementation, and constraint satisfaction. Moreover, [40] compares the performance of classical optimisation and soft computing algorithms when solving reconfiguration problems of power distribution systems. It was concluded that classical optimisation algorithms perform better than soft computing algorithms for small and medium-size systems (i.e., 33-bus and 136-bus, respectively).

Combining the optimisation model with the receding horizon framework, the Model Predictive Control (MPC)-based EMS optimises forecasts of behaviour over a future time horizon, which leads the system to act in advance of predicted future system changes [42,43]. EMSs

Table 1
Comparison of the proposed EMS with EMSs for EPSs on aircraft in other research.

Ref.	EMS methods	Multi-time scale	EPS complexity		Control targets*				Fault considerations		
			Single bus	Multi bus	PM	LM	RC	ESM	Single fault	Multiple faults	EMS internal communication fault
[18]	Deterministic rules	×	×	✓	✓	×	✓	×	✓	✓	×
[22]	FSM	×	✓	×	✓	✓	✓	✓	✓	✓	×
[30]	DP	×	✓	×	✓	×	×	✓	×	×	×
[33]	MIQP	×	✓	×	✓	×	×	✓	✓	×	×
[34]	NSGA-II	×	✓	×	✓	×	×	✓	×	×	×
[35]	NSGA-II	×	✓	×	✓	×	×	✓	×	×	×
[36]	PSO	×	×	✓	✓	×	×	×	×	×	×
[44]	MILP; MPC; Deterministic rules; Hierarchical control	✓	×	✓	✓	✓	✓	✓	✓	×	×
[45]	MILP; SMPC; Deterministic rules; Hierarchical control	✓	×	✓	✓	✓	✓	✓	✓	×	×
[46]	MIQP, MPC, distributed control	×	×	✓	✓	✓	✓	✓	×	×	×
[47,48]	MPC, nonlinear programming	×	✓	×	✓	×	×	✓	×	×	×
[49]	MPC	×	✓	×	✓	×	×	✓	×	×	×
[50]	NSGA-II, MPC, disconnection rules	×	✓	×	✓	×	×	✓	✓	×	×
[51]	MIQP, SMPC	×	×	✓	✓	✓	✓	✓	✓	✓	×
[55,56]	Two-level fuzzy rules	✓	✓	×	✓	×	×	✓	×	×	×
[57]	Two-level MPC	✓	✓	×	✓	×	×	✓	×	×	×
[58,59]	MIQP, MPC, Hierarchical control	✓	✓	×	✓	×	×	✓	×	×	×
[68]	Three-level fuzzy rules	✓	×	✓	✓	✓	×	×	✓	✓	×
This study	MILP, MPC, BR, FSM, Hierarchical control	✓	×	✓	✓	✓	✓	✓	✓	✓	✓

* In control targets, PM indicates power references; LM indicates load management; RC indicates reconfiguration; ESM indicates energy storage management.

targeting optimising power and load management of the EPS on an MEA are formulated using MILP in an MPC framework in [44,45]. In [46], the distributed tactical power control approach is combined with the MIQP-MPC model to reduce the cost of fuel consumption for an EPS on MEA, considering the increasing number of power electronic components used. In [47,48], MPC-based EMSs are proposed to reduce the fuel consumption of a hybrid aircraft propulsion system consisting of a gas turbine, an electric motor, and a battery. [47] adopts a classical nonlinear programming-based MPC strategy for the EMS, while [48] proposes a nonlinear MPC with a cross-entropy method for the EMS. Differing from the hybrid systems in [47–49] studies a hybrid battery-fuel cell power system, and proposes an MPC-based EMS to minimise the interval energy loss of the system. EPS faulty conditions are considered when designing MPC-based EMS for aircraft power systems in [50,51], and for ground power systems in [52,53]. In [50], power management solutions are provided by the NSGA-II-MPC controller to optimise electrical power system level efficiency. Although the faulty condition is updated in the proposed MPC framework, the system reconfiguration decisions are made by simple disconnection rules because the EPS adopts a simple single-bus architecture. In contrast, [51] presents a study for a more complex multi-bus EPS architecture. Reconfiguration decisions under faulty conditions on MEA are further optimized by adopting MIQP-MPC-based EMS when minimising the EPS overall operational costs with the consideration of demand side uncertainty. In [52], fault tolerance of renewable power sources is introduced in the MILP-MPC model for residential grids aiming to reduce electricity costs. However, the EMS response to EPS short-term changes and multiple faulty scenarios are unexplored. The fault detection and reconfiguration of a single bus microgrid is studied in [53], proposing a fault mitigation block before updating the LP-MPC based EMS to follow the pre-designed power references. However, this method is not applicable when the EPS architecture is complex and hard to decouple optimal reconfiguration and power scheduling decisions.

In the aforementioned studies, EMSs contain a single layer to provide all EPS decisions. Researchers in [54] argue that control of systems with dynamics covering multiple time scales leads to a trade-off between control performance and computational effort if solved with a conventional single-layer MPC scheme. Hierarchical EMSs are widely adopted to achieve diverse-timescale control while adopting various algorithms,

benefiting from different control levels, which complement one another [16]. Hierarchical EMSs are proposed in studies of electric aircraft, electric vehicles, electric ships, and grids. In [55,56], a two-level fuzzy rule-based supervisory controller is designed for an MEA EPS, with the first level to determine the total required power, while the second level minimises the dissipated power and compensates for the slower dynamic behaviour of the ESS. In [57], the authors propose a two-level MPC-based EMS for an aircraft EPS, which supplies loads using hybrid power sources, to reduce long-term energy costs and transients in voltage and current regulation. Hierarchical MPC-based EMSs, modelled in MIQP, are developed for an aircraft electro-thermal system in [58] and an electro-mechano-thermal system in [59], to coordinate control decisions among different energy domains and optimise energy efficiency and dynamics. Studies in [54,60] propose a two-level MPC-based EMS for electric vehicles. To reduce hydrogen consumption for an electric vehicle in [54], the upper level optimises power trajectory and temperature, and the lower level optimises electrical power. In [60], the upper-level MPC optimises the battery capacity loss cost and battery cooling cost, and a lower-level MPC minimises the battery capacity loss cost. Three-layer EMSs are adopted for a hybrid power system on ships in [61], consisting of one DP-MPC controller to optimise the power scheduling of energy sources, one distributed controller to coordinate the differences in the characteristics of multiple energy sources, and one local controller to track the reference power. A similar EMS scheme is proposed in [62] for a hybrid DC microgrid, while the top layer applies optimisation without an MPC frame. For residential grids, two-level EMSs are widely adopted. [63,64] introduce a two-level home EMS to reduce daily household energy costs using the MPC-based HL and the rule-based LL controllers, hence compensating for the effects of forecast uncertainties and sample time resolution. In [65], the EMS contains an upper-level MPC targeting end-user cost minimisation, and a lower-level MPC maximising self-sufficiency and self-consumption of each local energy community. For networked microgrids, the high-level EMS proposed in [66] uses a blockchain model to manage transactions among microgrids, and the low-level EMS uses the grid synchronization algorithm to manage the interconnection of microgrids. In [67], a hierarchical EMS is proposed for a fuel cell-supercapacitor-lithium battery hybrid energy storage system to maximise the system recovery power. The upper level contains a maximum power operation mode and a state

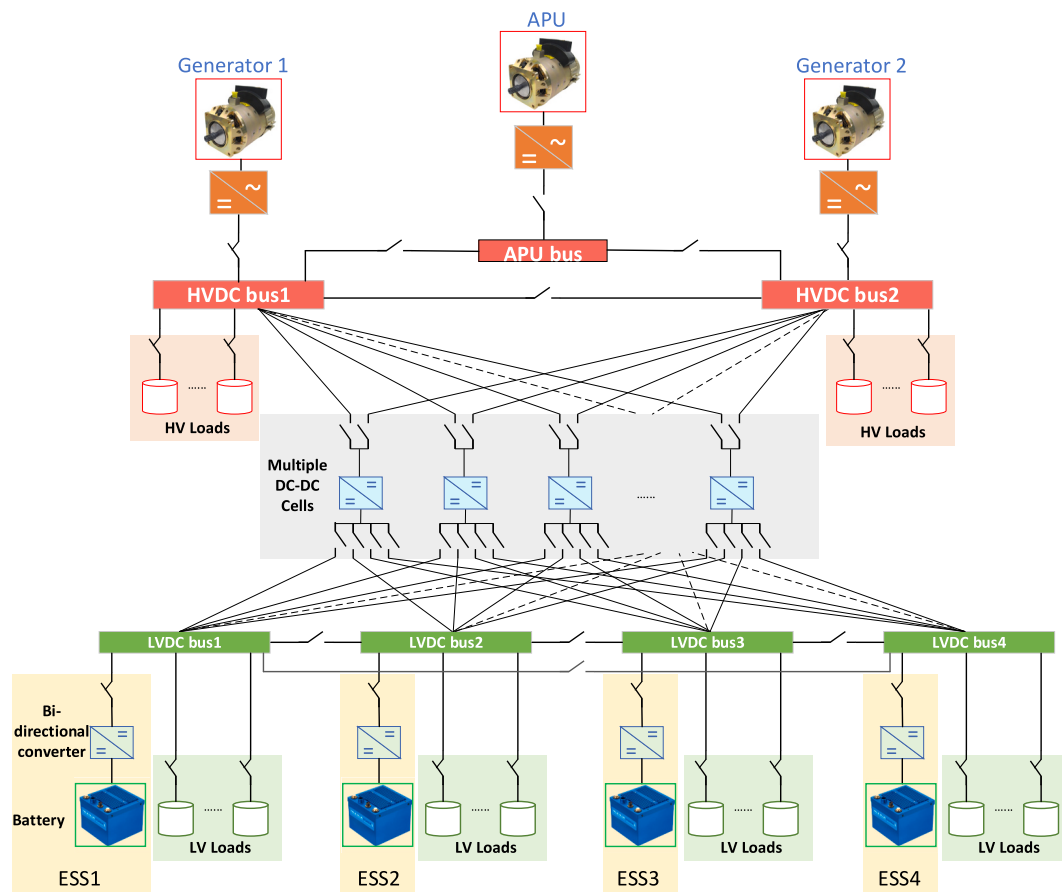


Fig. 1. An innovative EPS architecture for aircraft.

machine control algorithm operation mode, and the lower level adopts a fractional-order sliding mode controller to handle system nonlinear characteristics. However, none of the aforementioned studies explores the faulty scenarios of the EPS. Considering the load operative mode and health level of an MEA, a three-level hierarchical fuzzy rule-based EMS, consisting of a task level, an optimisation level, and a detection level, is studied in [68] for fault-tolerant load management. However, this study lacks reconfiguration decisions under multiple faulty component scenarios for the onboard EPS. In contrast, multiple faulty component scenarios are considered in [44,45]. A rule-based Low-Level (LL) controller is proposed to collaborate with an MPC-based High-Level (HL) controller in the EMS for an MEA EPS; however, the idea is relatively general without the LL controller design details. In addition, none of these mentions how the LL controller can operate when the online MPC in the HL controller is unavailable. Moreover, although a variety of EMS strategies are proposed for electric vehicles and grids, these studies lack the consideration of aircraft's particular safety and operational requirements, the methods proposed in these studies cannot be applied to aircraft EPSs.

1.3. Research gap and contribution

In summary, as presented in Table 1, although some studies propose EMSs for aircraft EPSs, there is little research on the multiple component faulty scenarios and the corresponding reconfigurations for the onboard EPS. In addition, in hierarchical EMS design studies, none mention the EMS internal reliability when considering the EMS internal communication faults. Furthermore, innovative multi-converter-based EPS architectures have recently attracted interest for future aircraft [51,69–71]. Compared to current studies in the literature, the coordinate design of a hierarchical EMS is more complex due to the growing

number of configuration requirements and nonlinearity in these architectures.

Motivated by the research gaps, this paper proposes an intelligent EMS containing a two-level hierarchical control framework for the innovative multi-converter-based onboard EPS, which is able to deal with multiple faulty scenarios, with optimisation. Table 1 presents the comparison of the proposed EMS to other state-of-the-art studies of EMSs for aircraft EPSs. This research considers EPS faulty scenarios resulting in system power shortage. These faulty scenarios include a) loss of one generator caused by bearing failure, short circuits, engine shut down, etc.; b) loss of batteries caused by a short circuit, poor connections, physical damage, etc.; c) loss of DC/DC converters caused by overvoltage/undervoltage conditions, short circuit, overheating, semiconductor wear-out, etc.; d) loss of transmission links caused by connector failure, short circuits, and wear and tear. A HL controller based on a MILP-MPC scheme is proposed to cope with the long-term optimisation of EPS operations, while an LL controller with a faster clock is designed to cope with load changes and fault occurrences over the short term within the HL sample intervals. This LL controller is designed based on a set of flight rules, which can work in both collaboration mode with the HL controller, or independent mode, when the online MPC at the HL is unavailable. The unavailable online MPC scenario is considered as an additional faulty condition within the EMS controller, which can be caused by communication faults at the online MPC input side or other real-time computation errors. The contributions of this research are as follows:

- 1) This research presents the mathematical formulation of a MILP-MPC model in the HL controller of an EMS. The model integrates nonlinear efficiency characteristics and discrete configuration limitations to calculate optimal power flow. In addition, varying weight

Table 2
EPS components' roles in normal and faulty operation cases.

EPS Component	EPS normal scenario	EPS faulty scenario
Generators/APU	Generators/APU are controlled based on voltage regulation to stabilise the HV/APU bus voltage. 1) HV/LV loads must be supplied. 2) The generator output power is used to charge the batteries according to the EMS.	1) In a generator failure scenario, the APU can be used to supply the loads and charge batteries. 2) The APU has a starting time of about 20s before it is available to be connected to the APU bus.
ESS	An ESS is used to stabilise the LV bus voltage for each LV bus. The ESS manages the power deviations between the loads and power transferred by cells.	ESSs can be used to supply LV loads when there is insufficient available power from the HV side caused by component failures.
HVBs to LVBs transmission links	One DC/DC cell can be connected to any HV or LV bus by controlling the on/off status of the contactors for power transmission.	By reconfiguring the system with redundant links, the LV side power shortage in transmission failure scenarios is mitigated.
HV/LV bus interconnections	The buses are isolated for aircraft safety reasons.	The bus interconnections are allowed to maintain bus voltage and supply critical loads.

factors are adopted in the objective functions of the MILP-MPC model to balance conflicting objectives, such as saving redundant energy in an ESS and reducing power losses by reduced power transmission. Moreover, offline MILP-MPC decisions are saved as a

database and available for complementary references when the online MILP-MPC is unavailable.

- 2) A rule-based LL controller is designed with four modes - two of the modes operate collaboratively when the online MILP-MPC is available to deal with EPS normal and failure scenarios, respectively, while the other two modes operate independently when the online MPC is unavailable. In each independent mode, an FSM-based algorithm is proposed in addition to a Basic Rule (BR)-based algorithm to improve the EMS performance in reducing continuous switching of charging/discharging of ESS and connection/disconnection of loads.
- 3) A comprehensive comparison study is conducted for two cases. The first case presents the EMS performance in the EPS normal operational scenario, with real-time load demand deviating from the ideal load prediction. The second case presents the EMS performance when assuming a series of component faults occur during the flight. In each case, the EMS in different modes and algorithms is simulated and compared, including BR-based independent LL control, FSM-based independent LL control, and collaborated HL and LL control. Hence, the effectiveness of the proposed EMS design can be proven.

1.4. Outline

The rest of this paper is organised as follows. [Section 2](#) introduces the EPS architecture and the hierarchical framework of EMS. [Section 3](#) presents the mathematical formulation of MILP-MPC for the HL controller of EMS, and [Section 4](#) demonstrates four modes of the LL controller. In [Section 5](#), simulation results for two case studies are compared. The paper is concluded in [Section 6](#).

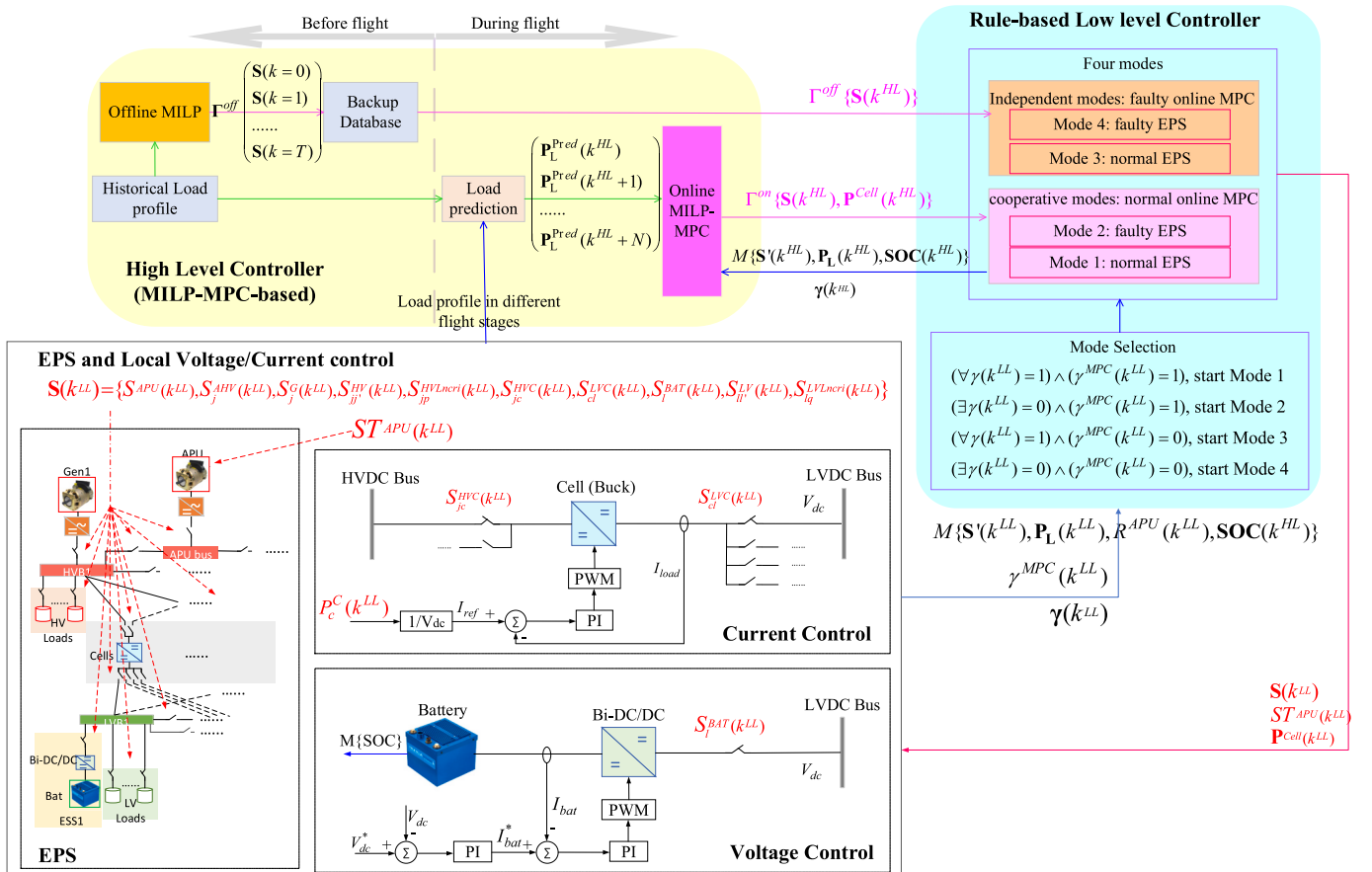


Fig. 2. The proposed hierarchical EMS.

Table 3
Control roles in each level.

Functions	LL controller roles	HL controller roles
Load management	Shed sufficient loads if a power shortage happens to keep critical loads being supplied	Online: Minimise load shedding and switching activities
EPS reconfiguration	Respond immediately to EPS component failures: 1) isolate faults 2) if needed, reconfigure the EPS by providing available connections based on EPS symmetry 3) consider APU starting duration for APU connection	Online: Provide configuration allowing minimum transmission power losses and switching activities in both normal and faulty scenarios Offline: Provide configuration allowing minimum transmission power losses and switching activities in normal scenarios, which can be referred to by the LL in EPS faulty scenarios to guide the optimisation
Power scheduling	Maintain instantaneous power balance and power limitations	Online: 1) Minimise transmission power losses 2) Maintain average power balance and power limitations
ESS management	Keep SOC within the limitations	Online: 1) Optimise ESS usage 2) Keep SOC within the desired limits

2. EPS architecture and hierarchical EMS framework

2.1. Electric power system

An innovative multi-converter-based EPS architecture is shown in Fig. 1, consisting of a 270 V HVDC network and a 28 V LVDC network, which is connected by multiple DC/DC power converters (named cells). The EPS normal scenario and the faulty scenario are defined according to the availability of the EPS components. Accordingly, the role of the system components will change in different cases to ensure the power supply requirements of the HV/LV loads are met. A detailed description of the EPS components/subsystems' roles is given in Table 2. In an MEA system, the onboard loads usually change according to different flight stages, including ground, take off, climb, cruise, descent, loiter, and landing [46]. Moreover, it is required to ensure aircraft critical loads, such as flight control systems, are supplied in all scenarios, while non-critical loads can be shed in faulty scenarios, when needed, following the load priorities. For example, an ice protection unit is obviously less preferred to be shed than an entertainment load.

2.2. Hierarchical EMS framework

The hierarchical framework proposed in this work includes two levels, as presented in Fig. 2. The LL control is conducted very quickly, every T_s^{LL} (i.e. 0.1 s). In contrast, the HL control is based on a slower clock T_s^{HL} (i.e. 1 min).

As presented in Fig. 2, the HL controller contains two decision-making parts. The first part is the online MILP-MPC, with the primary usage to provide power references of cells ($\mathbf{P}^{\text{Cell}}(k^{HL})$) and on/off statuses of all contactors ($\mathbf{S}(k^{HL})$) to the LL controller in the cooperative modes (Mode 3 and Mode 4). In the meantime, this online MILP-MPC takes the load predictions for the horizon, e.g. $\mathbf{P}_{Li}(k^{HL})$, $\mathbf{P}_{Li}(k^{HL} + 1)$, ..., $\mathbf{P}_{Li}(k^{HL} + N-1)$, as well as the system updates from the LL controller, into the online optimization calculations. The system updates include the realistic on/off status of all contactors ($\mathbf{S}'(k^{HL})$), all load power demands ($\mathbf{P}_L(k^{HL})$), the SOC of ESSs ($\mathbf{SOC}(k^{HL})$), and all EPS faulty information ($\gamma(k^{HL})$). The online optimization is multi-objective and gives an optimized control sequence for k^{HL} , $k^{HL} + 1$, ..., $k^{HL} + N-1$, where N indicates the total time steps contained in the finite prediction horizon H . However, only the first sample of the optimized control sequence is applied, and the horizon is shifted to the next time step $k^{HL} + 1$. This is known as the receding horizon. The second part is the backup database providing $\mathbf{S}(k^{HL})$ to the LL controller in the independent modes (Mode 1 and Mode 2) when the online strategy is unavailable because of real-time communication or computation failures. This backup database is generated before the flight by conducting an offline MILP optimisation

model similar to MILP-MPC, for all flight stages in the EPS normal scenario. This offline database aids the LL in decoupling the EPS reconfiguration problem (i.e., all connection decisions) from power flow calculations, which is essential in improving the feasibility of rules in the LL controller. Otherwise, determining the EPS configurations and power flows simultaneously results in nondeterministic rules in the LL controller, again increasing the unwanted computational complexity.

The proposed LL controller is based on predefined deterministic rules. It provides quick responses to maintain instantaneous power balance and capacity limitations, configure the EPS, and maintain critical loads even in faulty scenarios. As presented in Fig. 2, at each time step k^{LL} , the LL controller receives the real-time system status. In addition to the ones that will be sent to the HL controller (i.e., $\mathbf{S}'(k^{LL})$, $\mathbf{P}_L(k^{LL})$, $\mathbf{SOC}(k^{HL})$, and $\gamma(k^{LL})$), the availability status of the APU ($R^{APU}(k^{LL})$) and the availability of the online MILP-MPC ($\gamma^{\text{MPC}}(k^{LL})$) are also received. The LL controller will enter select one operation mode according to $\gamma^{\text{MPC}}(k^{LL})$ and $\gamma(k^{LL})$. Following the rules introduced in Section 4, the selected mode of the LL controller takes the recommendations from the HL controller into consideration, and then provides real-time decisions of $\mathbf{S}(k^{LL})$, $\mathbf{P}^{\text{Cell}}(k^{LL})$, and whether to start the APU ($ST^{APU}(k^{LL})$). The following gives the brief discussion of how the LL controller operates corresponding to the availability of the online MILP-MPC:

- 1) When the online MILP-MPC is available, during every time step k^{HL} , the LL controller receives recommendations $\Gamma^{\text{on}}\{\mathbf{S}(k^{HL}), \mathbf{P}^{\text{Cell}}(k^{HL})\}$ from the online MILP-MPC. It compares the recommendations with the real-time status information measured based on the fast clock T_s^{LL} , such as the faulty information of components and real-time load demands, to check the applicability of the recommendations to any EPS short-term behaviours. If the recommendation values are expected to lead to the power of components/links exceeding the limitations or resorting to the failed components, the LL controller adjusts the recommendation values to fit the real-time status; otherwise, the LL controller directly adopts the recommendation values and applies these to the EPS. The LL controller is in Mode 1 or Mode 2 when the EPS is in normal or faulty condition, respectively.
- 2) When the online MILP-MPC is unavailable, during every time step k^{HL} , the LL controller receives recommendations $\Gamma^{\text{off}}\{\mathbf{S}(k^{HL})\}$ from the offline database. In the EPS normal condition, the LL controller in Mode 3 calculates power references for the cells ($\mathbf{P}^{\text{Cell}}(k^{LL})$) based on the configuration extracted from the database. In EPS faulty scenarios, the LL controller in Mode 4 reconfigures the system by referring to the configuration in the database. Although the

configuration references cannot be directly applied to the EPS, rules are defined in the LL controller to calculate the potential symmetric available connections. Therefore, the LL controller provides the EPS with a new configuration ($\mathbf{S}(k^{LL})$) to resolve the power shortage caused by failures. Accordingly, power references for the cells ($\mathbf{P}^{\text{Cell}}(k^{LL})$) are calculated based on this updated configuration.

As shown in Fig. 2, real-time decisions of $\mathbf{S}(k^{LL})$ are directly applied to the contactors in the EPS. Each cell is using current control which takes the corresponding power reference from $\mathbf{P}^{\text{Cell}}(k^{LL})$ as the input of the control loop. For the components controlled under voltage control, their power is indirectly controlled because they are required to compensate for the power balance. Table 3 summarizes the fundamental roles for each control level.

3. High-level controller in EMS

This section presents the optimisation model, using MILP within the online MPC framework. The HL database is also constructed by solving this model offline.

3.1. Objective functions

For optimal operation management of the EPS, a multi-objective cost function (1) is formed, combining all of the individual cost functions introduced in (2)–(9), with different weighting factors w_{psupply} , w_{SOC} , w_{SL} , $w_{\delta\text{APU}}$, $w_{\delta\text{tran}}$, $w_{\delta\text{L}}$, w_{pGMAX} , and w_{Δ} correspondingly. Cost function (2) aims to minimise total power consumption from all power sources, resulting in lower power losses for the power distribution system, which consequently leads to lower fuel consumption. Cost function (3) aims to maximise the energy stored in the ESS, within the target range, thereby being prepared for abnormal conditions which may later require stored power. Cost function (4) aims to minimise the load shedding, following the load priorities. Cost functions (5)–(7) aim to minimise the switching activities to avoid unnecessary transients and contactor wear that can negatively affect the components' lifetimes. In (5)–(7), \mathbf{S}^{tran} denotes the vector of all power transmission line switches, i.e. $[S_j^{\text{AHV}}, S_{jj}^{\text{HV}}, S_{jc}^{\text{HVC}}, S_{cl}^{\text{LVC}}, S_l^{\text{BAT}}, S_l^{\text{LV}}]$. Similarly, \mathbf{S}^{L} denotes the vector of all load switches, i.e. $[S_{jp}^{\text{HVLncr}}, S_{jq}^{\text{LVLncr}}]$. Cost function (8) aims to minimise the generator sizing. The last cost function (9) aims to minimise the time for which SOC is outside of the target range, to coordinate with the soft constraints in Section 3.2.2.

$$J_{\text{MO}} = w_{\text{psupply}} J_{\text{psupply}} + w_{\text{SL}} J_{\text{SL}} + w_{\delta\text{APU}} J_{\delta\text{APU}} + w_{\delta\text{tran}} J_{\delta\text{tran}} + w_{\delta\text{L}} J_{\delta\text{L}} + w_{\text{SOC}} J_{\text{SOC}} + w_{\Delta} J_{\Delta} + w_{\text{pGMAX}} J_{\text{pGMAX}} \quad (1)$$

$$J_{\text{psupply}} = \sum_{k^{HL}=0}^{N-1} \left(\frac{\left(\sum_j^{N^{\text{HVB}}} P_j^{\text{G}}(k^{HL}) + P^{\text{APU}}(k^{HL}) \right)}{N^{\text{G}} \bullet P^{\text{Gmax}}} + \frac{\sum_l^{N^{\text{LV}}} P_l^{\text{dis}}(k^{HL})}{N^{\text{BAT}}} \right) \quad (2)$$

$$J_{\text{SOC}} = \sum_{k^{HL}=0}^{N-1} \frac{\sum_l^{N^{\text{LV}}} |HI - \text{SOC}_l(k^{HL})|}{N^{\text{BAT}} \bullet HI} \quad (3)$$

$$J_{\text{SL}} = \sum_{k^{HL}=0}^{N-1} \frac{\sum_j^{N^{\text{HVB}}} \sum_p^{N^{\text{HVLncr}}} \lambda_{jp}^{\text{HVLncr}} \left(-S_{jp}^{\text{HVLncr}}(k^{HL}) \right) + \sum_l^{N^{\text{LV}}} \sum_p^{N^{\text{LVLncr}}} \lambda_{jp}^{\text{LVLncr}} \left(-S_{jp}^{\text{LVLncr}}(k^{HL}) \right)}{\sum_j^{N^{\text{HVB}}} \sum_p^{N^{\text{HVLncr}}} \lambda_{jp}^{\text{HVLncr}} + \sum_l^{N^{\text{LV}}} \sum_p^{N^{\text{LVLncr}}} \lambda_{jp}^{\text{LVLncr}}} \quad (4)$$

$$J_{\delta\text{APU}} = \sum_{k^{HL}=0}^{N-1} |S^{\text{APU}}(k^{HL} + 1) - S^{\text{APU}}(k^{HL})| \quad (5)$$

$$J_{\delta\text{tran}} = \sum_{k^{HL}=0}^{N-1} \sum |S^{\text{tran}}(k^{HL} + 1) - S^{\text{tran}}(k^{HL})| \quad (6)$$

$$J_{\delta\text{L}} = \sum_{k^{HL}=0}^{N-1} \sum |S^{\text{L}}(k^{HL} + 1) - S^{\text{L}}(k^{HL})| \quad (7)$$

$$J_{\text{pGMAX}} = \sum_{k^{HL}=0}^{N-1} \frac{P^{\text{Gmax}}(k^{HL})}{P^{\text{MAXG}}} \quad (8)$$

$$J_{\Delta} = \sum_{k^{HL}=0}^{N-1} \sum_l^{N^{\text{LV}}} (\varepsilon_l(k^{HL}) + \vartheta_l(k^{HL})) \quad (9)$$

Among the objectives, increasing SOC and reducing the power losses are two conflicting objectives, because charging batteries to increase SOC causes additional power losses. However, their importance changes in different conditions: when the SOC is close to the upper bound, reducing the power losses can be more prioritized than increasing SOC; whereas, when the SOC is close to the lower bound, improving EPS safety by charging the battery is more important, regardless of the consequent power losses. A varying SOC weighting factor is therefore designed in (10) to balance the energy redundancy and power losses, where $w_{\text{soc}}^{\text{max}}$ and $w_{\text{soc}}^{\text{min}}$ are the maximum and minimum weights selected for the varying SOC.

$$w_{\text{soc}_i}(k) = w_{\text{soc}}^{\text{min}} + \frac{\text{SOC}_i(k=0) - LO}{HI - LO} (w_{\text{soc}}^{\text{max}} - w_{\text{soc}}^{\text{min}}) \quad (10)$$

3.2. Constraints

To demonstrate the EPS operational requirements, six groups of constraints are proposed, which are briefly discussed here. More details have been discussed in our studies in [13,51,72,73].

3.2.1. Power balance constraints

For each bus node, the power flows should comply with the rule that the sum of powers flowing into/out of each node equals zero. For the converter nodes, the power flowing out of each node is less than the power flowing into it because of the nonlinear converter efficiency, which is here linearised using piecewise functions [73]. In addition, power losses across the transmission lines are considered by adding a constant transmission efficiency parameter to the model. For all of the bidirectional power flows, the power in each direction is represented by a separate non-negative variable, hence all power variables here are non-negative.

1) Power balance formulation for each APU bus node:

$$P^{\text{APU}}(k^{HL}) - \sum_j^{N^{\text{HVB}}} P_j^{\text{AHVp}}(k^{HL}) + \sum_j^{N^{\text{HVB}}} \eta_j^{\text{AHV}} P_j^{\text{AHVn}}(k^{HL}) = 0 \quad (11)$$

2) Power balance formulation for each HV bus nodes:

$$P_j^G(k^{HL}) + \left(\eta_j^{AHV} P_j^{AHVp}(k^{HL}) - P_j^{AHVn}(k^{HL}) \right) + \left(\sum_{j \neq j'} \left(\eta_{jj'}^{HV} P_{jj'}^{HV}(k^{HL}) - P_{jj'}^{HV}(k^{HL}) \right) \right) - \sum_c^{N^C} P_{jc}^{HVC}(k^{HL}) - \sum_p^{N^{HVLcri}} P_{jp}^{HVLcri}(k^{HL}) - \sum_p^{N^{HVLncr}} S_{jp}^{HVLncr}(k^{HL}) P_{jp}^{HVLncr}(k^{HL}) = 0 \quad (12)$$

3) Power balance formulation for each Cells' node:

$$\eta_c \sum_j^{N^{HVB}} \eta_{jc}^{HVC} P_{jc}^{HVC}(k^{HL}) - \sum_l^{N^{LVB}} P_{cl}^{LVC}(k^{HL}) = 0, \forall c \in \{1, \dots, N^C\} \quad (13)$$

4) Power balance formulation for all LV bus nodes:

$$\sum_c^{N^C} \eta_{cl}^{LVC} P_{cl}^{LVC}(k^{HL}) + \sum_{l \neq l'} (\eta_{ll'}^{LV} P_{ll'}^{LV}(k^{HL}) - P_{ll'}^{LV}(k^{HL})) + (P_l^{dis}(k^{HL}) - P_l^{ch}(k^{HL})) - \sum_q^{N^{LVLcri}} P_{lq}^{LVLcri}(k^{HL}) - \sum_q^{N^{LVLncr}} S_{lq}^{LVLncr}(k^{HL}) P_{lq}^{LVLncr}(k^{HL}) = 0, \forall l \in \{1, \dots, N^{LVB}\} \quad (14)$$

3.2.2. ESS constraints

For each battery (in an ESS), the SOC at time step $k^{HL}+1$ can be estimated from the battery power and SOC value at the previous time step k^{HL} , as shown below, where $\forall l \in \{1, \dots, N^{LVB}\}$.

$$SOC_l(k^{HL}+1) = SOC_l(k^{HL}) + \frac{T_s \eta_l^{ch} P_l^{ch}(k^{HL})}{B_l^{cap}} - \frac{T_s P_l^{dis}(k^{HL})}{\eta_l^{dis} B_l^{cap}}, \forall l \in \{1, \dots, N^{LVB}\} \quad (15)$$

In the aircraft system, SOC is preferred to be kept within a target range [LO, HI]. In this work, LO = 0.3 and HI = 0.9 are considered. As mentioned in [72], soft constraints in (16)–(18) are proposed to improve the robustness of the MILP-MPC algorithm, which allows SOC to vary slightly outside of this range in real situations due to unpredicted power requirements.

$$0.3 - \varepsilon_l(k^{HL}) \leq SOC_l(k^{HL}) \leq 0.9 + \vartheta_l(k^{HL}), \forall l \in \{1, \dots, N^{LVB}\} \quad (16)$$

$$0 \leq \varepsilon_l(k^{HL}) \leq 0.1 \quad (17)$$

$$0 \leq \vartheta_l(k^{HL}) \leq 0.1 \quad (18)$$

3.2.3. Boundary constraints

Each component and transmission link has a maximum power limit for safe operation. For the potential unidirectional power flow, when its physical transmission path is connected, the power should not exceed its limit, otherwise, the power is restricted to zero. Similarly, for the potential bidirectional power flow, the power is limited by the direction indicator, i.e., only the selected power direction can reach its maximum power limitation. This set of constraints is presented in (19), where S indicates the matrix of physical connection and direction indicators, P indicates the matrix of corresponding power flow, and P_{max} indicates the power flow to each element in P .

$$0 \leq P(k^{HL}) \leq S(k^{HL}) \times P_{max} \quad (19)$$

As mentioned in [13], the maximum power of each generator and

APU can be restricted during the flight by introducing the following power limitation constraints.

$$0 \leq P^{Gmax}(k^{HL}) \leq S_j^G(k^{HL}) \bullet P^{MAX^G}, P_j^G(k^{HL}) \leq P^{Gmax}(k^{HL}), P^{APU}(k^{HL}) \leq P^{Gmax}(k^{HL}) \quad (20)$$

3.2.4. Unidirectional constraints

For the potential bidirectional power flow, two non-negative variables are introduced to present the power flow in each direction. (21) and (19) indicate that when the physical transmission link is connected, the power can be transferred in either direction within the given maximum value. Additionally, when the physical transmission link is disconnected, power flow in both directions is set to zero. In (19), s^p and s^n indicates a matrix of the power direction indicators for the link, allowing bidirectional power flow, and S^{phy} indicates the matrix of the physical connentions of these links.

$$s^p(k^{HL}) + s^n(k^{HL}) \leq S^{phy}(k^{HL}) \quad (21)$$

3.2.5. Connection constraints of operation restrictions

The power contactors should be connected properly to provide the system with all possible operation topologies and prevent unexpected connection conditions. The connection constraints are proposed for APU connection, buses interconnections, and the cells' connections as follows:

1) The APU is connected to the APU bus only when any of the main generators fails:

$$S^{APU}(k^{HL}) \leq \left(1 - \prod_j^{N^{HVB}} \gamma_j^G(k^{HL}) \right) \quad (22)$$

2) The HV and APU bus interconnections are only allowed when any generator failure occurs. HV buses and the APU bus should also be connected without creating loops:

$$\sum_j^{N^{HVB}} S_j^{AHV}(k^{HL}) + S_{jj'}^{HV}(k^{HL}) \leq N^{HVB} \bullet \left(1 - \prod_j^{N^{HVB}} \gamma_j^G(k^{HL}) \right) \quad (23)$$

$$\sum_j^{N^{HVB}} S_j^G(k^{HL}) + S^{APU}(k^{HL}) + \sum_j^{N^{HVB}} S_j^{AHV}(k^{HL}) + S_{jj'}^{HV}(k^{HL}) \leq N^{HVB} + N^{APU} \quad (24)$$

3) Each HV bus should be supplied by only one healthy power source, either one main generator or the APU:

$$1 \leq S_j^G(k^{HL}) + S_j^{AHV}(k^{HL}) + S_{jj}^{HV}(k^{HL}) \leq 2, \forall j \in \{1, \dots, N^{HVB}\} \quad (25)$$

4) Although the cells are flexible enough to be connected with any HV/LV bus, during the system operation, each cell cannot be connected to more than one HV and one LV bus:

$$0 \leq \sum_j S_{jc}^{HVC}(k^{HL}) \leq 1, \forall c \in \{1, \dots, N^C\} \quad (26)$$

$$0 \leq \sum_l S_{cl}^{LVC}(k^{HL}) \leq 1, \forall c \in \{1, \dots, N^C\} \quad (27)$$

5) The LV bus interconnections are only allowed when any battery failure occurs. LV buses should be connected without creating loops:

$$\sum_l S_{il}^{LV}(k^{HL}) \leq (N^{BAT} - 1) \left(1 - \prod_j \gamma_j^{BAT}(k^{HL}) \right) \quad (28)$$

$$\sum_l S_l^{BAT}(k^{HL}) + \sum_l S_{il}^{LV}(k^{HL}) \leq N^{BAT} \quad (29)$$

6) Each LV bus should be supplied by only one healthy battery, to maintain the bus voltage:

$$1 \leq S_{i(l-1)}^{BAT}(k^{HL}) + S_{i(l-1)}^{LV}(k^{HL}) + S_{i(l+1)}^{LV}(k^{HL}) \leq 2, \forall l \in \{1, \dots, N^{LVB}\} \quad (30)$$

3.2.6. Health status constraints for components in EPS

A component can only be connected when it is available, as presented in (31), where $S_{\alpha,\beta}$ indicates the connection β to any component α in the system, γ_α indicates the availability of any component α .

$$S_{\alpha,\beta}(k^{HL}) \leq \gamma_\alpha(k^{HL}) \quad (31)$$

4. Low-level controller in EMS

In each mode, a group of rules are defined to work as an expert system to either collaborate with online MPC (Mode 1 and 2) or supervise the system independently (Mode 3 and 4). In the independent modes, two different rule-based methods are proposed, i.e. BR and FSM.

4.1. LL mode 1: collaboration mode in EPS normal scenarios

Algorithm I is proposed for the LL in Mode 1, which adopts the recommendations of the HL for configurations and load shedding, and calculates the power references based on the load power deviations using the following rules:

- Power Rule 1:** If the ESS for LV bus l can compensate for the deviations between predicted and real-time loads, then adopt recommended power references for cells connected to bus l .
- Power Rule 2:** If the battery is over-charged when adopting the HL-recommended power of cells which are connected with LV bus l , then reduce the power of the corresponding cells proportionally based on the HL recommendations.
- Power Rule 2:** If the battery is over-discharged when adopting the HL-recommended power of cells which are connected with LV bus l , then increase the power of the corresponding cells proportionally based on the HL recommendations.

Algorithm I for LL Mode 1

Algorithm I for LL Mode 1

- Consider system state at time step k^{LL}
 - Load power measurement: $P_{jp}^{HVLcri}(k^{LL})$, $P_{jp}^{HVLncri}(k^{LL})$, $P_{lq}^{LVLcri}(k^{LL})$, $P_{lq}^{LVLncri}(k^{LL})$
- Keep MPC controller recommendation of system configuration references and load shedding: $S^{conf}(k^{LL}) = \Gamma^{on}\{S^{conf}(k^{HL})\}$, $S^{shed}(k^{LL}) = \Gamma^{on}\{S^{shed}(k^{HL})\}$
- Calculate power references $P^C(k^{LL})$ to control the battery charging/discharging and load supporting:

For each LV bus l , do the following:

 - Calculate the deviations $P_l^{LVdev}(k^{LL})$ between the recommended input power from cells and real-time load demands, as presented in (32)

$$P_l^{LVdev}(k^{LL}) = \sum_{c=1}^{N^C} P_{cl}^{LVC}(k^{HL}) - \sum_{q=1}^{N^{LVLcri}} P_{lq}^{LVLcri}(k^{LL}) - \sum_{q=1}^{N^{LVLncri}} S_{lq}^{LVLncri}(k^{LL}) \cdot P_{lq}^{LVLncri}(k^{LL}) \quad (32)$$
 - Calculate the power capacity remained from cells to the LV bus l , i.e. $P_{cl}^{LVcrem}(k^{HL})$, when recommended power references were allocated, as presented in (33)

$$P_{cl}^{LVcrem}(k^{HL}) = P_{cl}^{LVCmax} \cdot S_{cl}^{LVC}(k^{LL}) - P_{cl}^{LVC}(k^{HL}) \quad (33)$$
 - If** $-P_l^{dismax} \leq P_l^{LVdev}(k^{LL}) \leq P_l^{chmax}$ **Then Apply Power Rule 1** as below

$$P_{cl}^{LVC}(k^{LL}) = P_{cl}^{LVC}(k^{HL})$$
 - If** $P_l^{LVdev}(k^{LL}) > P_l^{chmax}$ **Then Apply Power Rule 2** as (34)

$$P_{cl}^{LVC}(k^{LL}) = P_{cl}^{LVC}(k^{HL}) \cdot \left(1 - \frac{(P_l^{LVdev}(k^{LL}) - P_l^{chmax})}{\sum_{c=1}^{N^C} P_{cl}^{LVC}(k^{HL})} \right) \quad (34)$$
 - If** $P_l^{LVdev}(k^{LL}) < -P_l^{dismax} < 0$ **Then Apply Power Rule 3** as (35)

$$P_{cl}^{LVC}(k^{LL}) = P_{cl}^{LVC}(k^{HL}) - \frac{P_{cl}^{LVcrem}(k^{HL})}{\sum_{c=1}^{N^C} P_{cl}^{LVcrem}(k^{HL})} \cdot (P_l^{LVdev}(k^{LL}) + P_l^{dismax}) \quad (35)$$
- Obtain updated control references for the system: $S^{conf}(k^{LL})$, $S^{shed}(k^{LL})$, $P^C(k^{LL})$, the cells' power is calculated by (36)

$$P^C(k^{LL}) = \sum_l S_l^{LVB} P_{cl}^{LVC}(k^{LL}) \quad (36)$$

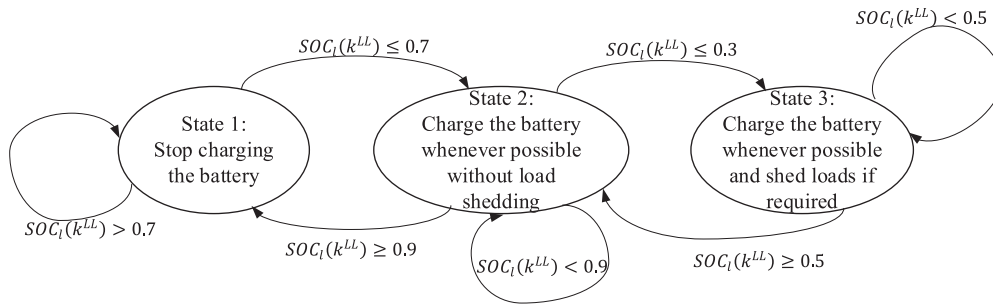


Fig. 3. FSM-based mode 3.

Table 4

Predicted load profile of power usage (kW) based on flight stages.

Load types [kW]	Ground (20 min)	Take off (5 min)	Climb (25 min)	Cruise (60 min)	Descent (10 min)	Loiter (15 min)	Landing (15 min)
Critical Loads on each HV bus	3.34	9.86	7.40	7.15	7.40	9.07	10.00
Critical Loads on LV bus 1 and 4	1.78	1.94	2.07	3.00	2.07	2.07	1.94
Critical Loads on LV bus 2 and 3	3.00	2.50	2.50	2.50	2.50	2.50	3.00
High Priority Loads on each HV bus	1.63	2.78	8.00	8.00	8.00	8.00	0.29
High Priority Loads on LV bus 1 and 4	1.40	1.30	1.30	1.30	1.60	0.80	0.80
High Priority Loads on LV bus 2 and 3	0.50	0.50	0.50	0.50	1.50	1.00	2.20
Mid Priority Loads on each HV bus	5.00	1.14	4.72	4.87	4.72	4.72	1.14
Mid Priority Loads on LV bus 1 and 4	0.50	0.35	0.35	2.00	0.35	0.35	0.35
Mid Priority Loads on LV bus 2 and 3	0.70	0.70	1.50	2.50	0.50	0.50	0.50
Low Priority Loads on each HV bus	2.00	2.00	2.00	6.00	2.00	2.00	2.00
Low Priority Loads on LV bus 1 and 4	1.00	0.70	1.50	2.20	0.50	0.50	1.50
Low Priority Loads on LV bus 2 and 3	2.00	1.50	2.00	3.00	2.00	2.00	2.00

Table 5

Weights for the evaluation indices.

V_{glass}	2	V_{SOC}	$W_{soc}^{max} = 2, W_{soc}^{min} = 0$
V_{SL}	50	$V_{\delta APU}$	4
V_{stran}	1	$V_{\delta L}$	8
V_{pmuc}	0.2	$V_{\delta pbat}$	0.4
$V_{violation}$	100		

4.2. LL mode 2: collaboration mode in EPS faulty scenarios

Algorithm II is proposed for the LL in mode 2. In Algorithm II, the initial configuration decisions adopt the online MPC recommendations. When the recommendations are applicable, the configuration decisions remain unchanged. Otherwise, the following configuration rules are applied to update decisions when MPC has yet to respond to failures, and the recommendations are not applicable. The configuration rules are achieved by Boolean logical operations.

- Configuration Rule 1:** Interconnect HV buses when a single generator/APU needs to supply more than one HV bus, including the APU starting period.
- Configuration Rule 2:** APU is started if high-priority and mid-priority loads should be shed caused by the generator failure and the delay in the MPC response.
- Configuration Rule 3:** Before the online MPC responds to the generator failure, shed sufficient loads if needed to avoid the overload of the generator.

- Configuration Rule 4:** Isolate the faulty battery and connect the neighbour LV bus to maintain the LV bus voltage.
- Configuration Rule 5:** Before the online MPC responds to the failures, the LL controller uses symmetric links and disconnects the faulty links and cells to maintain EPS safety and avoid power shortage as a very quick response, considering the left side and the right side of the EPS are symmetric.

Power rules are proposed in Algorithm II to work out LV load shedding $S_{lq}^{LVIncri}(k^{LL})$ considering all faulty scenarios, and calculate the power references $P^C(k^{LL})$ to control the battery charging/discharging and load supply.

- Power Rule 1 & 2:** Similar to Power Rules 1 & 2 in LL Mode 1, with the configuration updated following the configuration rules.
- Power Rule 3:** If the battery is over-discharged in real-time, and the over-discharge can be avoided by increasing the cells' power, then increase the power of the corresponding cells proportionally with the configuration updated following the configuration rules.
- Power Rule 4:** If the battery is over-discharged in real-time, but the over-discharge cannot be avoided by increasing the cells' power, then two actions should be taken: 1) Cells connected with the LV bus l are set to rated power; 2) Sufficient LV loads are shed to avoid the battery discharge exceeding the limitation following the load priority, as presented in Algorithm II-Shed-L.

Algorithm II. for LL Mode 2

Algorithm II for LL Mode 2

- 1) Consider system state at time step k^{LL}
 - a) system health status $\mathbf{y}(k^{LL})$
 - b) Load power measurement: $P_{jp}^{HVLncr}(k^{LL}), P_{jp}^{HVLncr}(k^{LL}), P_{lq}^{LVLncr}(k^{LL}), P_{lq}^{LVLncr}(k^{LL})$
 - c) APU availability status: $R^{APU}(k^{LL})$
- 2) Receive online MPC recommendations of system configuration references and load shedding: $\Gamma^{on}\{\mathbf{S}^{conf}(k^{HL})\}$ and $\Gamma^{on}\{\mathbf{S}^{shed}(k^{HL})\}$ as initial values for $\mathbf{S}^{conf}(k^{LL})$ and $\mathbf{S}^{shed}(k^{LL})$
- 3) Update system configuration $\mathbf{S}^{conf}(k^{LL})$ based on $\mathbf{y}(k^{LL})$ and $\Gamma^{on}\{\mathbf{S}^{conf}(k^{HL})\}$ by using **Configuration Rule 1-5**
- 4) Decide the LV side load shedding $S_{lq}^{LVLncr}(k^{LL})$ and calculate the power references $\mathbf{P}^C(k^{LL})$:

For each LV bus l (or set of connected buses, noting that when the LV bus l is connected to the LV bus l' , the two buses are regarded as a new combined single bus l), do the following:

- a) Calculate the power deviation $P_l^{LVdev}(k^{LL})$ between the recommended available input power and real-time load demands when adopting the EPS configuration $\mathbf{S}^{conf}(k^{LL})$ in (37)

$$P_l^{LVdev}(k^{LL}) = \sum_{c=1}^{N^C} P_{cl}^{LVC}(k^{HL}) \cdot S_{cl}^{LVC}(k^{LL}) \cdot \sum_{j=1}^{N^{HVB}} S_{jc}^{HVC}(k^{LL}) - \sum_{q=1}^{N^{LVLncr}} P_{lq}^{LVLncr}(k^{LL}) - \sum_{q=1}^{N^{LVLncr}} S_{lq}^{LVLncr}(k^{LL}) \cdot P_{lq}^{LVLncr}(k^{LL}) \quad (37)$$

- b) Calculate the power capacity remained from the cells to the LV bus l , i.e. $P_{cl}^{CLVrem}(k^{HL})$, when available recommended power references which were allocated and the EPS configuration $\mathbf{S}^{conf}(k^{LL})$ decided in step 3) is adopted, as presented in (38).

$$P_{cl}^{CLVrem}(k^{HL}) = P_{cl}^{LVCmax} \cdot S_{cl}^{LVC}(k^{LL}) \cdot \sum_{j=1}^{N^{HVB}} S_{jc}^{HVC}(k^{LL}) - P_{cl}^{LVC}(k^{HL}) \quad (38)$$

- c) **If** $-P_l^{dismax} \leq P_l^{LVdev}(k^{LL}) \leq P_l^{chmax}$ **Then Apply Power Rule 1** as below

$$P_{cl}^{CLV}(k^{LL}) = P_{cl}^{CLV}(k^{HL}) \cdot S_{cl}^{LVC}(k^{LL}) \cdot \sum_{j=1}^{N^{HVB}} S_{jc}^{HVC}(k^{LL})$$

- d) **If** $P_l^{LVdev}(k^{LL}) > P_l^{chmax}$ **Then Apply Power Rule 2** as (39)

$$P_{cl}^{LVC}(k^{LL}) = P_{cl}^{LVC}(k^{HL}) \cdot S_{cl}^{LVC}(k^{LL}) \cdot \sum_{j=1}^{N^{HVB}} S_{jc}^{HVC}(k^{LL}) \cdot \left(1 - \frac{P_l^{LVdev}(k^{LL}) - P_l^{chmax}}{\sum_{c=1}^{N^C} P_{cl}^{LVC}(k^{HL}) \cdot \sum_{j=1}^{N^{HVB}} S_{jc}^{HVC}(k^{LL})}\right) \quad (39)$$

- e) **If** $P_l^{LVdev}(k^{LL}) < -P_l^{dismax} < 0$ and $|P_l^{LVdev}(k^{LL}) + P_l^{LVdismax}(k^{LL})| \leq P_l^{CLVrem}(k^{LL})$ **Then Apply Power Rule 3** as (40)

$$P_{cl}^{LVC}(k^{LL}) = P_{cl}^{LVC}(k^{HL}) \cdot S_{cl}^{LVC}(k^{LL}) \cdot \sum_{j=1}^{N^{HVB}} S_{jc}^{HVC}(k^{LL}) + \frac{P_{cl}^{CLVrem}(k^{HL}) \cdot (-P_l^{LVdev}(k^{LL}) - P_l^{dismax})}{\sum_{c=1}^{N^C} P_{cl}^{CLVrem}(k^{HL})} \quad (40)$$

- f) **If** $P_l^{LVdev}(k^{LL}) < -P_l^{dismax} < 0$ and $|P_l^{LVdev}(k^{LL}) + P_l^{LVdismax}(k^{LL})| > P_l^{CLVrem}(k^{HL})$ **Then Apply Power Rule 4** as follows

i. Set Cells to rated power, i.e. $P_{cl}^{CLV}(k^{LL}) = P_{cl}^{LVCmax} \cdot S_{cl}^{LVC}(k^{LL}) \cdot \sum_{j=1}^{N^{HVB}} S_{jc}^{HVC}(k^{LL})$.

ii. Shed sufficient loads by adopting **Algorithm II-Shed-LVL**

Algorithm II-Shed-LVL Load shedding for LV bus l

Start from low-priority LV load $q = N^{LVLncr}$

While $q \geq 1$, Do the following calculation for LV bus l :

$$S_{lq}^{LVLncr}(k^{LL}) = 0$$

IF $P_l^{LVLtot}(k^{LL}) \leq P_l^{LVinmax}(k^{LL}) + P_l^{dismax}$, Break **While**;

Else $q = q - 1$;

End While

In Algorithm II-Shed-LVL, $P_l^{LVinmax}(k^{LL})$ indicates the maximum available input power from the HV side to l , $P_l^{LVLtot}(k^{LL})$ indicates the total power demand in on bus l .

$$P_l^{LVinmax}(k^{LL}) = P_{cl}^{LVCmax} \sum_c \eta_{cl}^{LVC} S_{cl}^{LVC}(k^{LL}) \cdot \sum_{j=1}^{N^{HVB}} S_{jc}^{HVC}(k^{LL}) \quad (41)$$

$$P_l^{LVLtot}(k^{LL}) = \sum_q P_{lq}^{LVLncr}(k^{LL}) + \sum_q S_{lq}^{LVLncr}(k^{LL}) P_{lq}^{LVLncr}(k^{LL}) \quad (42)$$

- 5) Obtain updated control references for the system: $\mathbf{S}^{conf}(k^{LL})$, $\mathbf{S}^{shed}(k^{LL})$, $\mathbf{P}^C(k^{LL})$, the cells' power is calculated by (36)

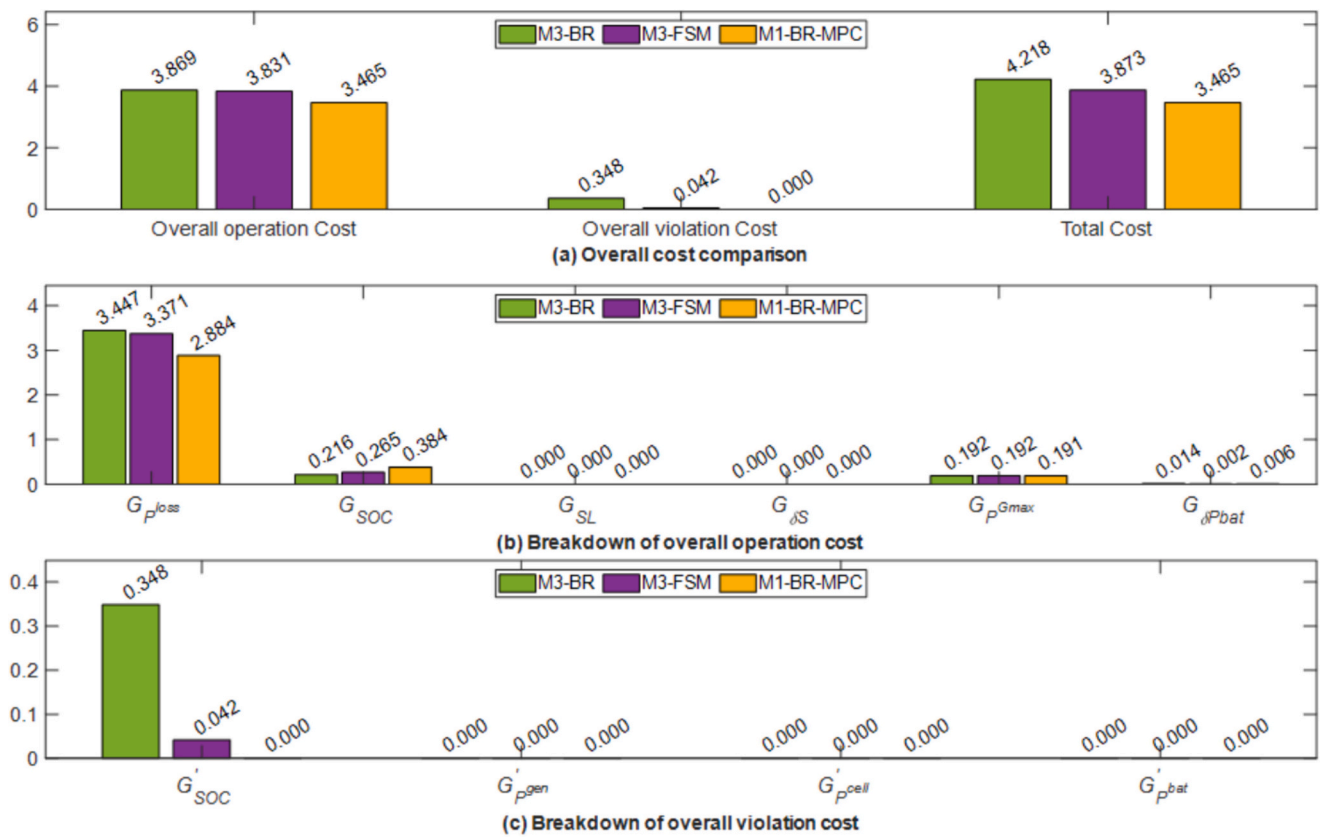


Fig. 4. Cost comparison of different controls without load deviations in EPS normal condition.

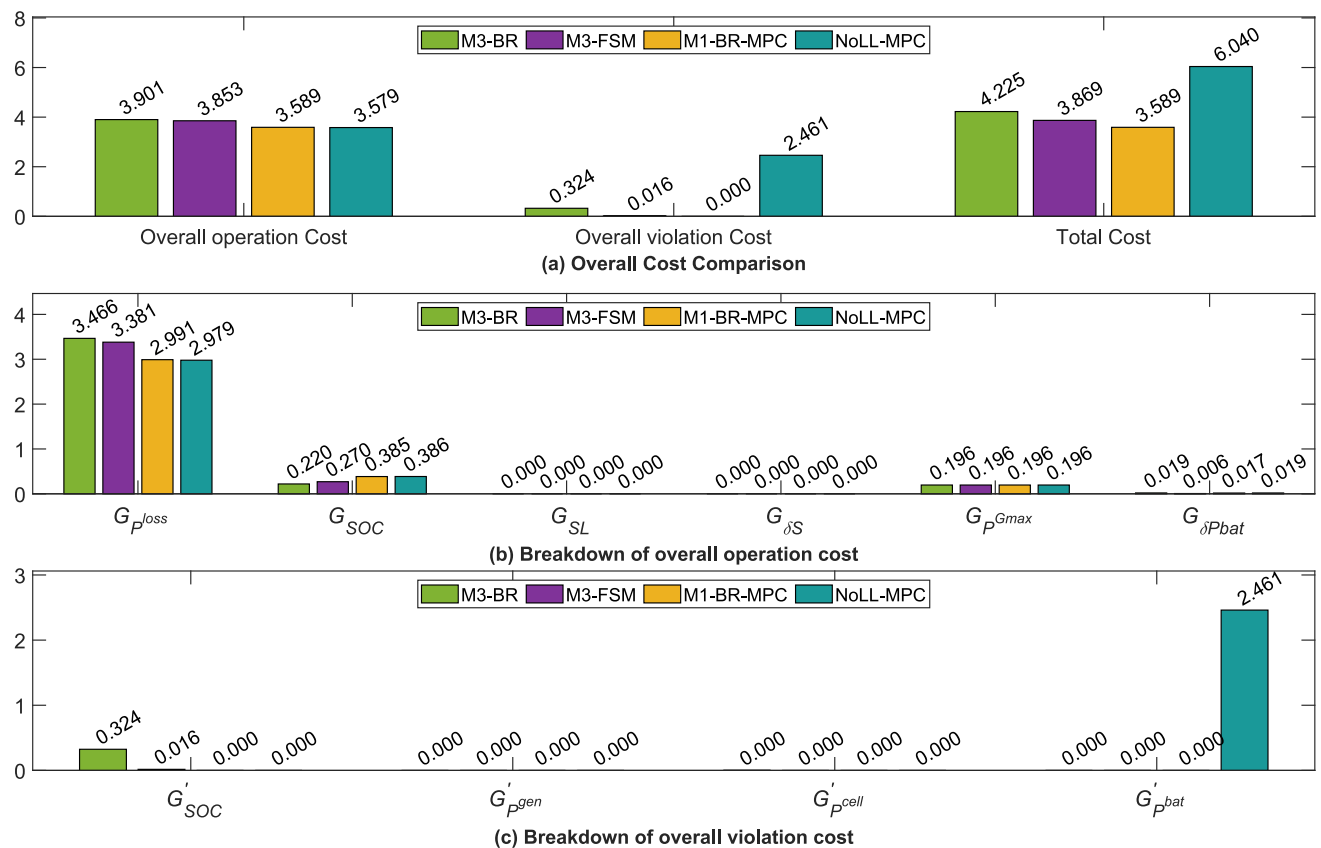


Fig. 5. Cost comparison of different controls with maximum load deviations in EPS normal condition.

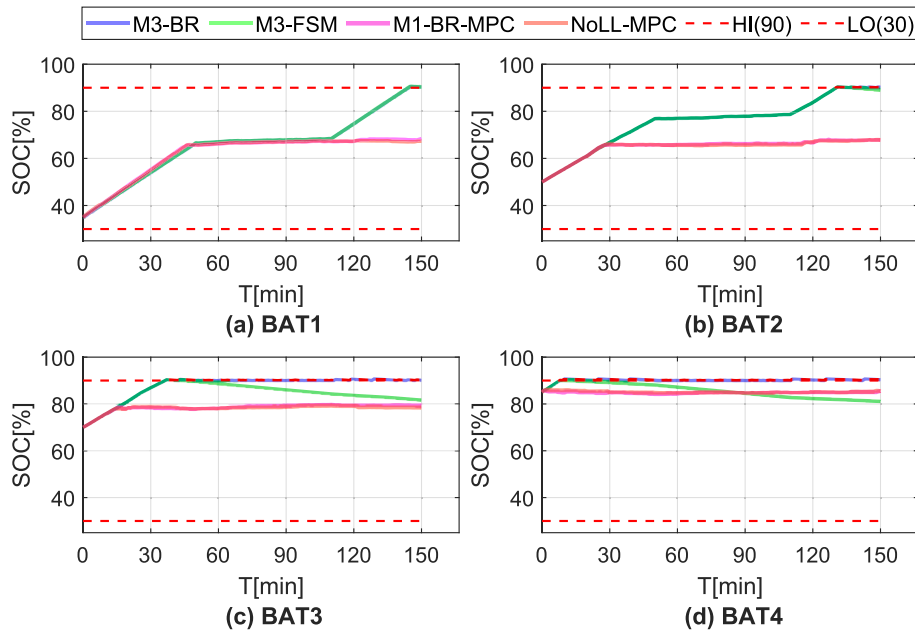


Fig. 6. SOC changes in Case 1.

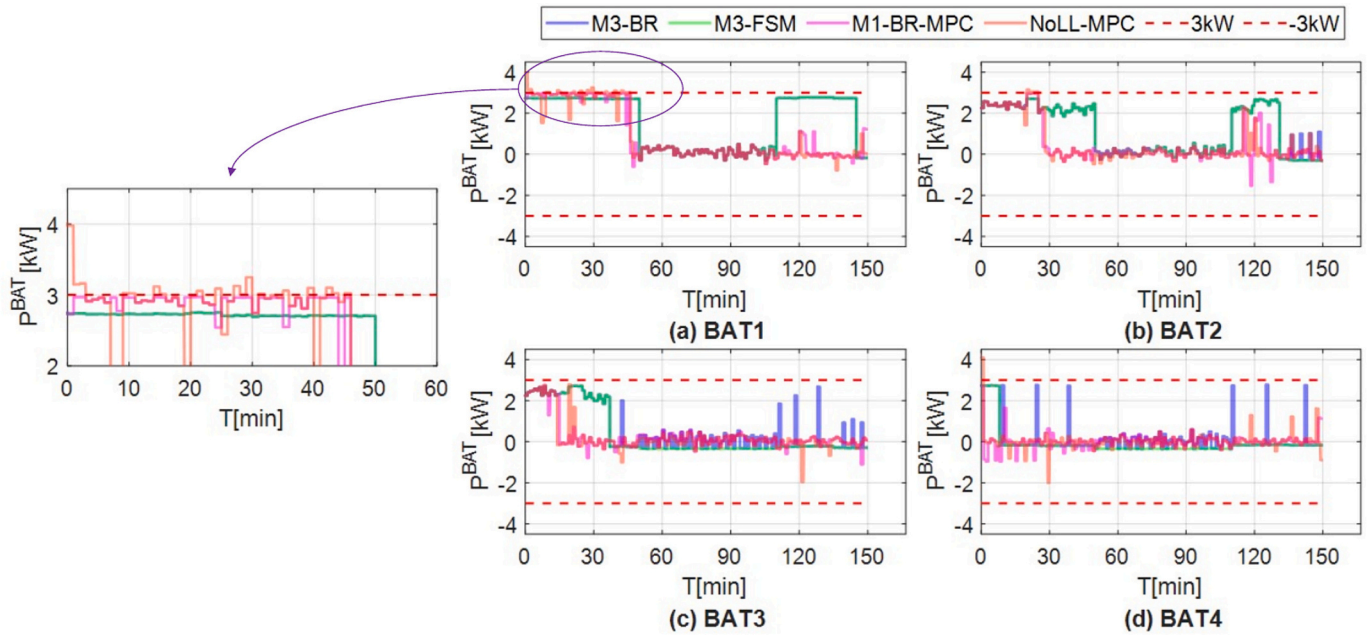


Fig. 7. Battery charging/discharging power in Case 1.

4.3. LL mode 3: independent mode in EPS normal scenarios

When the EPS is operating normally but the online MPC is unavailable, the LL in Mode 3 adopts the recommendations for configurations $\Gamma^{off} \{S^{conf}(k^{HL})\}$ from the backup database during each time interval T_s^{HL} . Both BR and FSM methods are proposed in the following subsections for comparison in Mode 3.

4.3.1. BR method for mode 3

Algorithm III is proposed for LL Mode 3 to calculate power references and decide load shedding according to three power rules:

- a) **Power Rule 1:** If SOC exceeds the upper bound, then stop charging the battery by sharing LV loads among cells equivalently within the cells' power capacity.
- b) **Power Rule 2:** If SOC is within the target range, then charge the battery whenever possible without load shedding by sharing LV

loads and charging power among cells equivalently within the cells' power capacity.

- c) **Power Rule 3:** If SOC exceeds the lower bound, then charge the battery whenever possible, otherwise, shed sufficient loads to charge the battery if required. When load shedding is required, shed sufficient loads following the load priorities.

Algorithm III for LL BR-based Mode 3

4.3.2. FSM method for mode 3

In Algorithm III, the battery can be quickly charged to its upper bound. However, the battery SOC is likely to vary around the upper bound because the battery keeps switching between the charging and discharging process, which leads to additional power losses and unnecessary power changes, and can be harmful to the battery lifetime. Compared to the BR method, which makes decisions based on the inputs,

Algorithm III for LL BR-based Mode 3

- 1) Consider system state at time step k^{LL}
 - a) Load power measurement: $P_{jp}^{HVLcri}(k^{LL}), P_{jp}^{HVLncri}(k^{LL}), P_{lq}^{LVLcri}(k^{LL}), P_{lq}^{LVLncri}(k^{LL})$
 - b) SOC measurement: $SOC_i(k^{LL})$
- 2) Read the dataset to extract system configuration references: $S^{conf}(k^{LL}) = \Gamma^{off}\{S^{conf}(k^{HL})\}$
- 3) Initially, set all loads as being connected, $S^{shed}(k^{LL}) = \mathbf{1}$
- 4) Calculate power references $P^C(k)$ and shed loads if required to control the battery charging/discharging and load supporting:

For each LV bus l , do the following:

 - a) Calculate the maximum available input power from HV side to LV bus l : $P_l^{LVinmax}(k^{LL})$ in (41)
 - b) Calculate the total load demands $P_l^{LVLtot}(k^{LL})$, as presented in (42)
 - c) **If $SOC_l(k^{LL}) \geq 0.9$ Then Apply Power Rule 1** as (43)

$$P_{cl}^{LVC}(k^{LL}) = \min(P_{cl}^{LVCmax}, P_l^{LVLtot}(k^{LL}) / \sum_c^{Nc} S_{cl}^{LVC}(k^{LL})) \cdot S_{cl}^{LVC}(k^{LL}) \quad (43)$$
 - d) **If $0.3 \leq SOC_l(k^{LL}) < 0.9$ Then Apply Power Rule 2** as (44)

$$P_{cl}^{LVC}(k^{LL}) = \min(P_{cl}^{LVCmax}, (P_l^{LVLtot}(k^{LL}) + P_l^{chmax}) / \sum_c^{Nc} S_{cl}^{LVC}(k^{LL})) \cdot S_{cl}^{LVC}(k^{LL}) \quad (44)$$
 - e) **If $(SOC_l(k^{LL}) < 0.3)$ Then Apply Power Rule 3** as follows
 - i. When $P_l^{LVLtot}(k^{LL}) \leq P_l^{LVinmax}(k^{LL})$, conduct (44)
 - ii. When $P_l^{LVLtot}(k^{LL}) > P_l^{LVinmax}(k^{LL})$, conduct **Algorithm II-Shed-LVL** until $P_l^{LVLtot}(k^{LL}) \leq P_l^{LVinmax}(k^{LL})$
- 5) Obtain updated control references for the system: $S^{conf}(k^{LL}), S^{shed}(k^{LL}), P^C(k^{LL})$, the cells' power is calculated by (36)

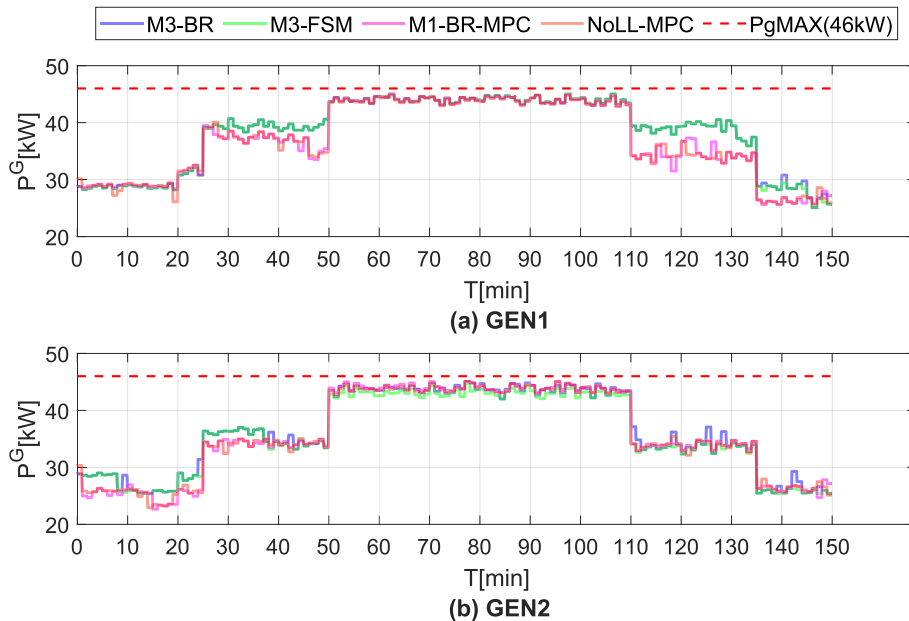


Fig. 8. Generator power in Case 1.

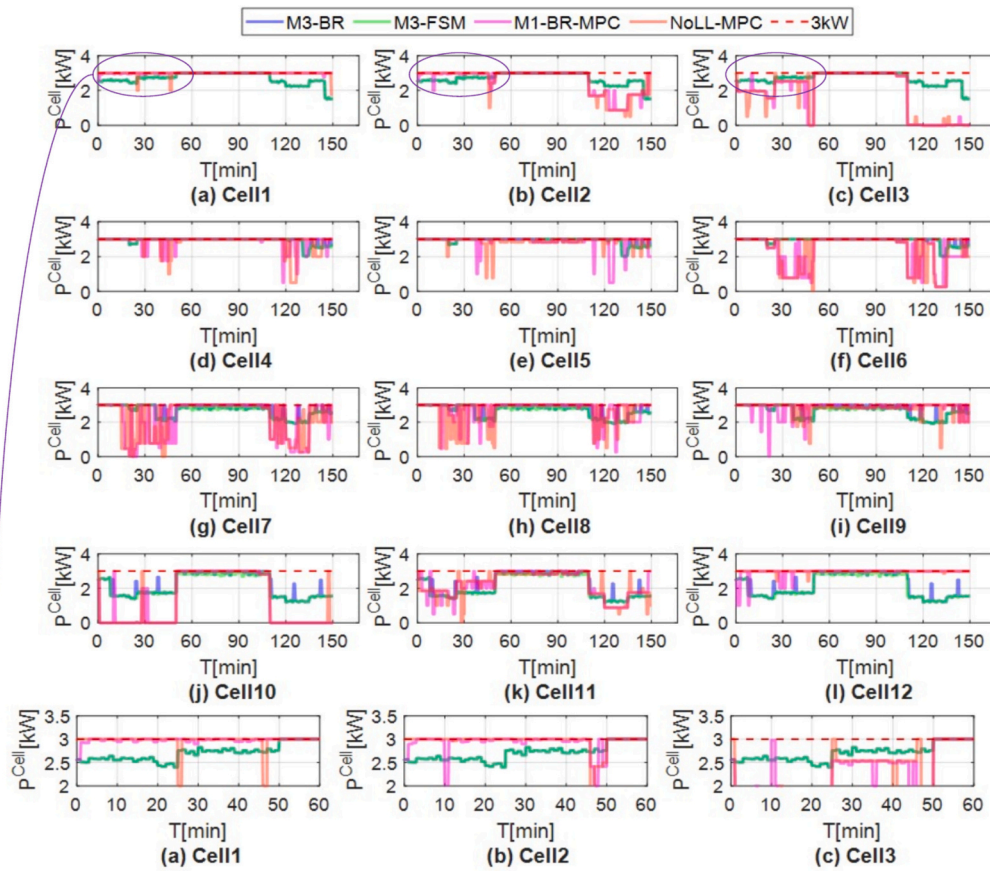


Fig. 9. Cells' input power for Case 1

Table 6
Failure events during the flight.

Instant of fault occurrence	1000s (16.67 min)	2000s (33.33 min)	3000 s (50 min)	4000 s (66.67 min)	5000 s (83.33 min)
Failed Component	Battery 4	Cell 10	Generator 1	S_{27}^{shc}	S_{11}^{sch}

the FSM decides outputs and the next state as a function of the inputs and the present state (allowing it to take the current state / previous decisions into consideration). To remove the continuous switching of charging/discharging in Algorithm III, FSM-based Mode 3 in Fig. 3 is proposed, which consists of three states and a group of state transition conditions. The controller continuously compares the inputs, i.e. the SOC of each battery, with the transition conditions. When a transition condition is satisfied, the controller transits from the present state to the next state to calculate the decision variables.

4.4. LL mode 4: independent mode in EPS faulty scenarios

In faulty scenarios, although the online MPC is unavailable to provide optimized recommendations for the failures, the LL can adopt rules to configure the EPS. The configuration rules in Mode 4 are similar to the ones in Mode 2. In addition, similarly to Mode 3, Mode 4 calculates the power in the EPS to manage loads and ESS to meet the operational constraints when the EPS configurations are decided, with BR-based and FSM-based methods proposed. Compared to Mode 3, load shedding is also conducted when there is a power shortage caused by failures when applying Power Rule 1–3 in Mode 3. Considering the similarity between the configuration rules between Mode 4 and Mode 2, as well as the power rules between Mode 4 and Mode 3, Algorithms for Mode 4 will

not be presented in detail to minimise redundancy and maintain brevity in this paper.

5. Case studies

To compare the performances of the proposed hierarchical control with different EPS scenarios, two cases are studied by simulating the EPS and the controller in Simulink. The MILP model is solved using the Gurobi solver (an off-the-shelf solver for MILP problems). In Case 1, the EPS is in a normal condition, and the real-time loads are assumed with a maximum deviation within $\pm 5\%$ compared to the predictions. The performances are compared when the online MPC collaborates with the LL in Mode 1 (M1-BR-MPC), and when the LL acts independently in Mode 3 using BR (M3-BR) and FSM (M3-FSM). In addition, the performance is also compared when the online MPC operates without the LL (NoLL-MPC) to study the impact of the response delay. Case 2 explores the EMS performance when the EPS operates in faulty scenarios. The performance is also compared when the online MPC collaborates with the LL in Mode 2 (M2-BR-MPC), and with an independent LL in Mode 4, again comparing the BR (M4-BR) and FSM (M4-FSM).

Load demand prediction during the flight is essential for effective operation of the HL controller. There are several prediction methods that could be used to predict the load demands [74]. Researchers in [63] argue that using historical data for load prediction reduces dependence on additional communication technologies (i.e., no need for complex forecasting packages that require additional meteorological data), making the controller more reliable when there are communication problems. In addition, [46,75] show that aircraft load demand is highly related to the flight stages; hence, the load demand can be predicted from a typical load profile obtained from historical flight stages. Consequently, this research adopts a load profile which is related to

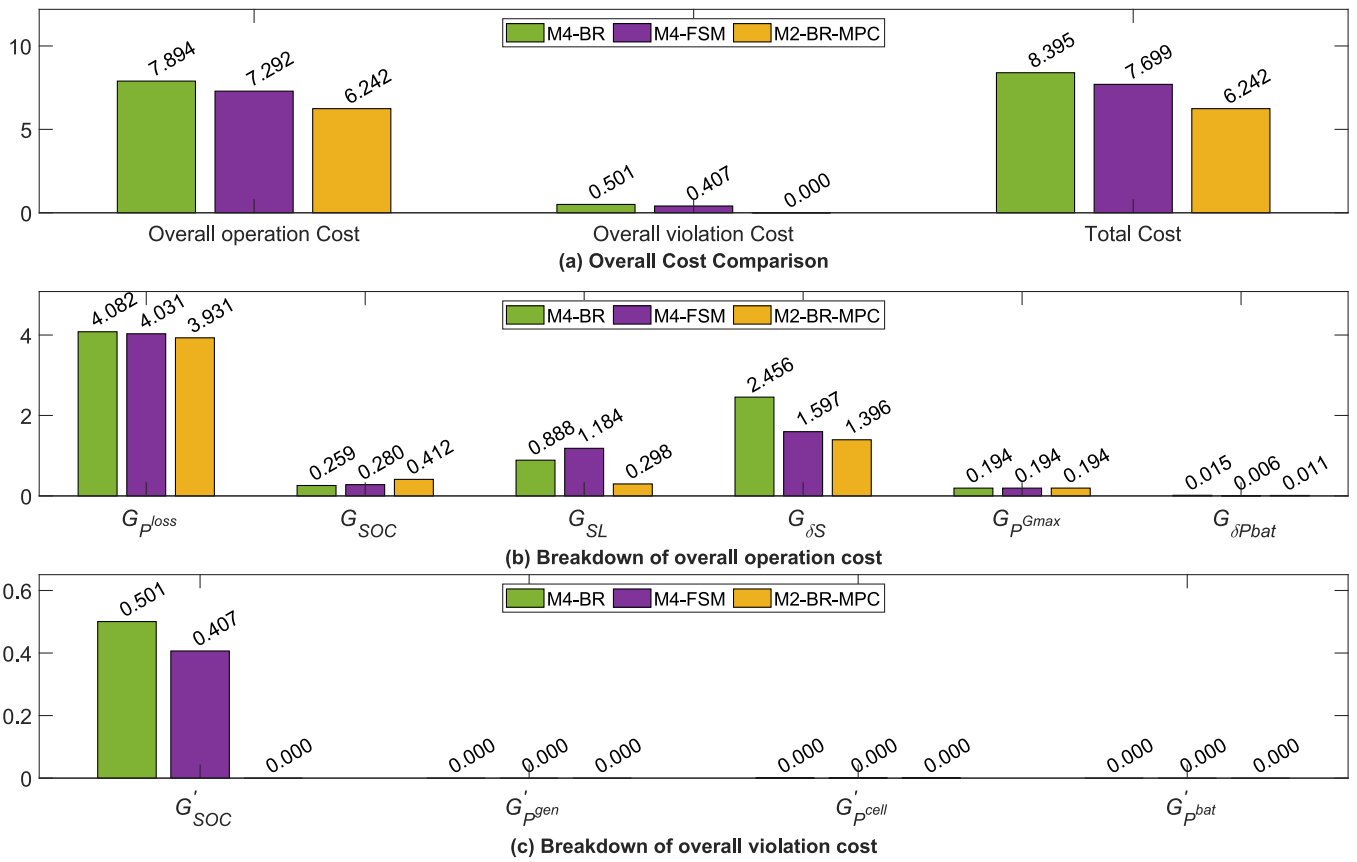


Fig. 10. Cost comparison of different controls for EPS faulty scenarios.

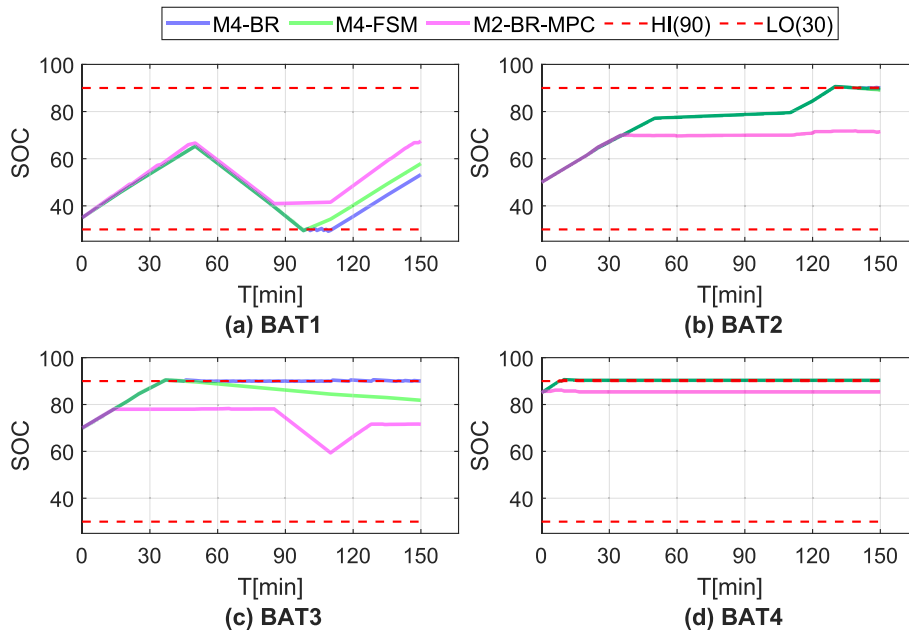


Fig. 11. SOC results for Case 2.

flight stages as the predicted load demands, referring to [46,51,76,77], as presented in Table 4. Moreover, uncertainties during the flight may introduce some fluctuations to these demands. The following sections will present how the controller handles these fluctuations; allowing the impact of the imprecise load prediction to be mitigated. As mentioned above, a maximum $\pm 5\%$ load demand fluctuation is introduced to the load prediction in this research.

Regarding the other parameters in the EPS, the rated power for each DC/DC converter is 3 kW, and the capacity of each battery is 6 kWh. The maximum load power is 43.02 kW on the left/right side when the aircraft enters the cruising stage, while the rated generator power is 46 kW, which is designed to cover all of the MEA loads. During the simulation, different SOC initial values are set for the batteries in the EPS, such as 0.35, 0.5, 0.7, 0.75.

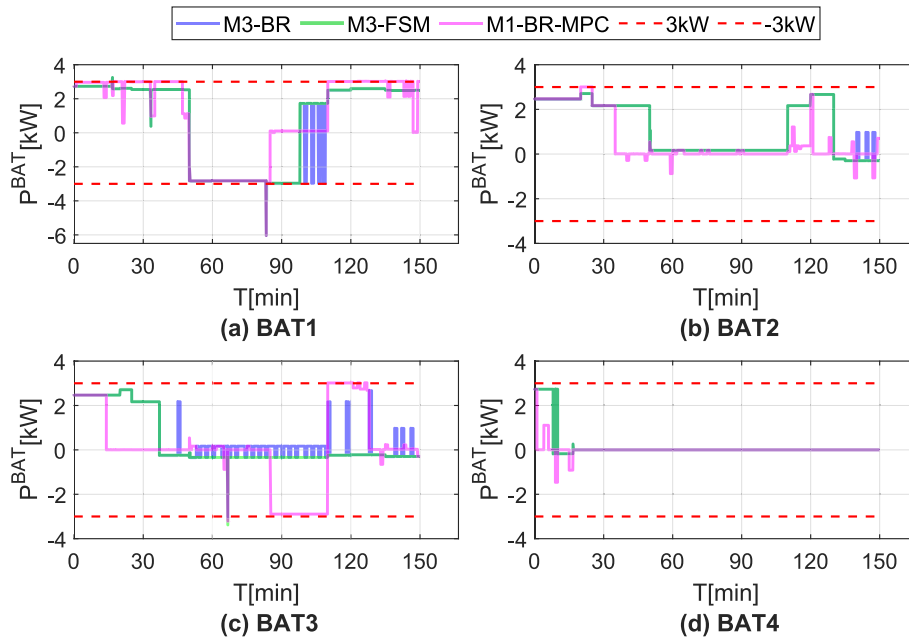


Fig. 12. Battery charging/discharging power for Case 2.

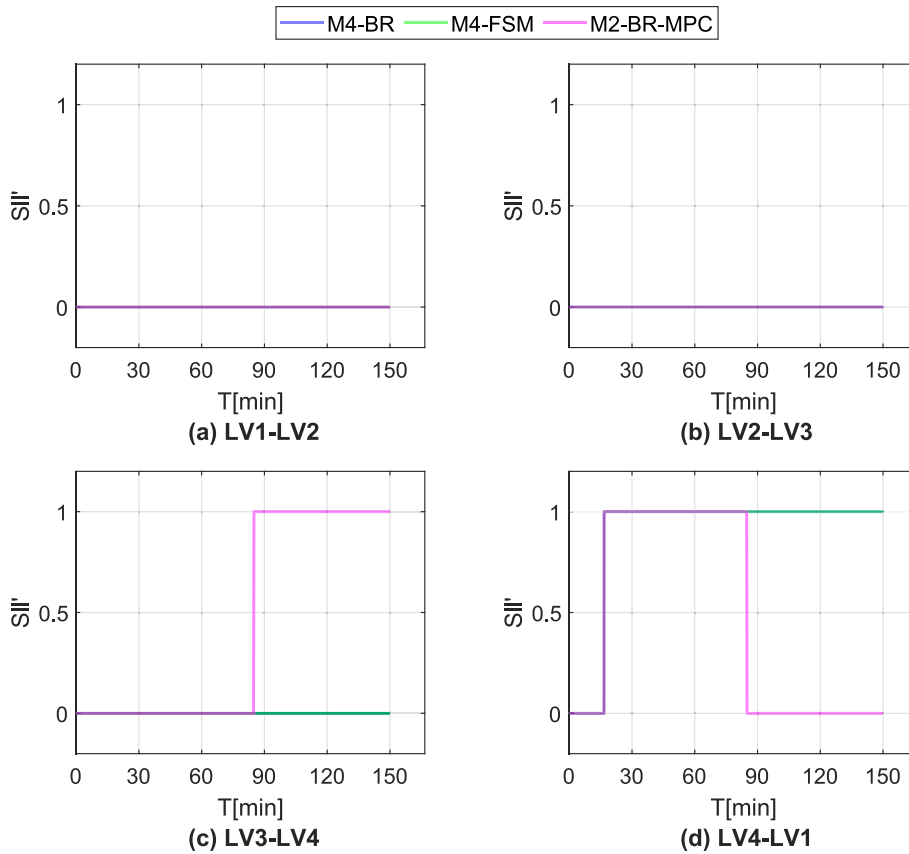


Fig. 13. LV bus connections for Case 2.

The performance of each method is estimated, considering operation costs and constraint violation costs. The operation costs (G_{op}) include power losses (G_{ploss}), SOC (G_{SOC}), load shedding (G_{SL}), switching (G_{δ}), maximum generator power (G_{pmax}), and battery power changes ($G_{\delta P_{bat}}$). The operation costs are calculated similarly to the objective functions in HL control. The constraint violation costs are evaluated by calculating

the average amount by which the values exceeded the target boundaries during the flight stages, for all corresponding components [51]. The violation costs (G'_{vio}) include the violation of the SOC target range (G'_{SOC}), the violation of the maximum power bounds for generator/APU output power (G'_{pgen}), and the violation of maximum power bounds for cells (G'_{pcell}) and battery power (G'_{pbat}). When calculating each cost value,

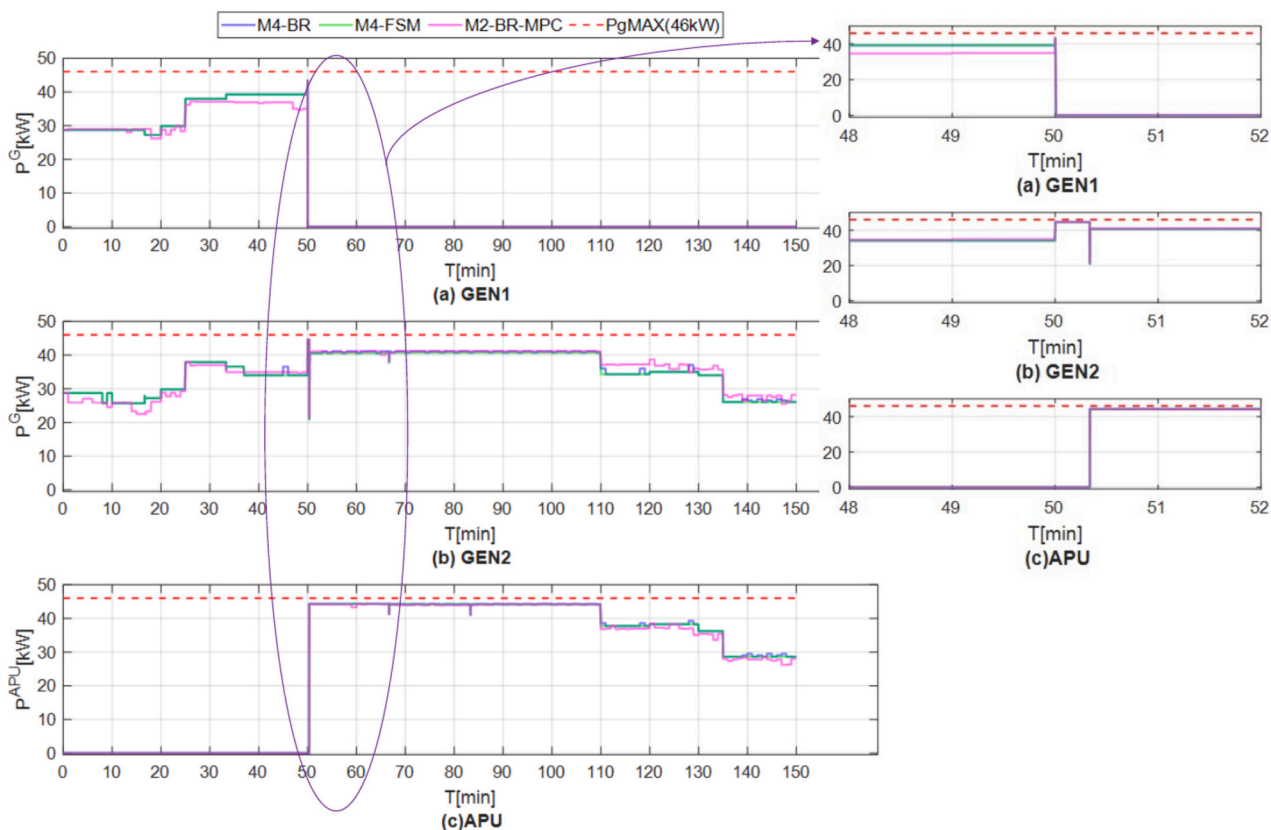


Fig. 14. Generator/APU output power for Case 2.

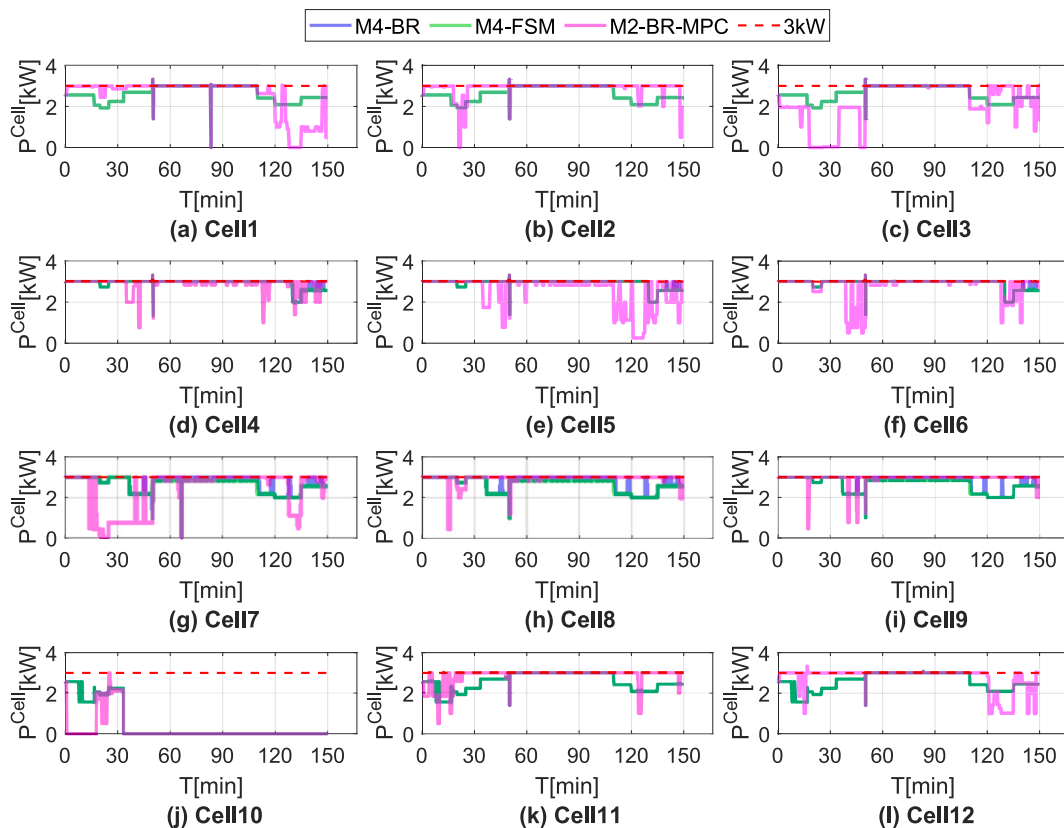


Fig. 15. Cells' input power for Case 2.

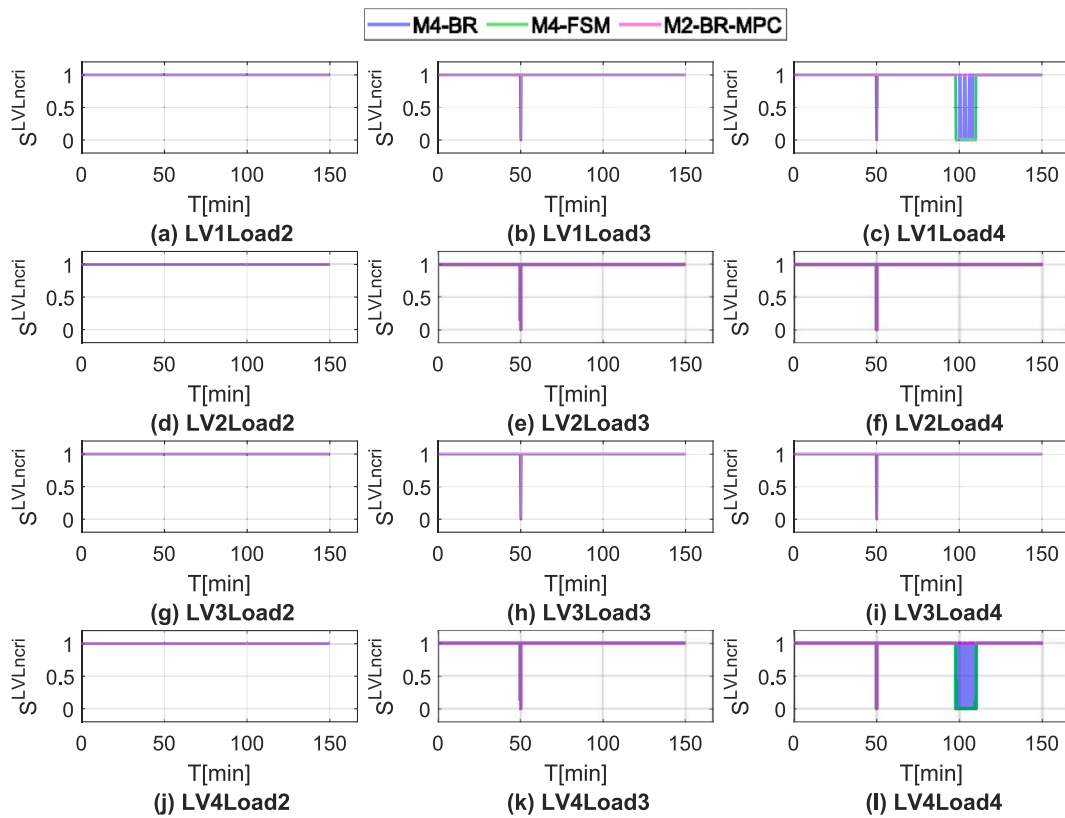


Fig. 16. Connection of LV non-critical loads on LV buses for Case 2.

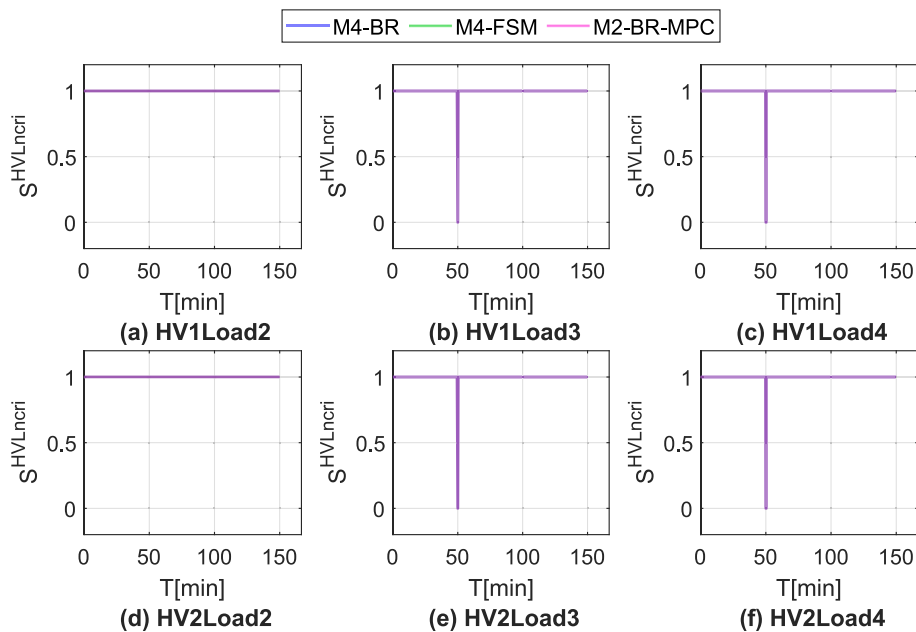


Fig. 17. Connection of HV non-critical loads on HV buses for Case 2.

the weighting factors in Table 5 are adopted considering the preference of various objectives referring to [72,78].

5.1. Case 1: EPS normal scenario

Fig. 4 presents the cost comparison with different methods when the loads are assumed to be as predicted, while Fig. 5 presents the comparison when the real-time loads are assumed to have the maximum ± 5

% deviations compared to the predicted values. Therefore, the impacts of the load deviations upon different proposed methods can be compared. In addition, the benefit of the LL control for dealing with real-time load changes is indicated by comparing the results for directly applying the recommendations of online MPC.

Fig. 4 (a) shows that the overall operation costs are much greater than the overall violation costs, and that violation costs vary a lot between approaches. M1-BR-MPC performs the best in minimising both

Table 7
Switching activities in Case 2.

	M4-BR	M4-FSM	M2-BR-MPC
δ_{APU}	1	1	1
δ_{trans}	13	13	15
δ_L	44	28	24

overall operation and violation costs. In addition, the overall violation cost is completely avoided when adopting M1-BR-MPC. Without the online MPC, M3-BR and M3-FSM perform similarly in terms of overall operation cost. However, M3-FSM performs better in reducing the overall violation cost compared to M3-BR. According to Fig. 4 (a), M1-BR-MPC reduces the overall operation cost by 10.45 % and 9.55 % and the total cost by 17.84 % and 10.62 %, compared to M3-BR and M3-FSM, respectively. Compared to M3-BR, M3-FSM reduces the total costs by 8.18 %.

Fig. 4 (b) breaks down the operation cost, showing that the majority of the operation costs are due to power losses. M1-BR-MPC leads to the minimum power loss and each generator output power. M3-FSM performs the best in reducing battery power changes, while M1-BR performs the best in SOC. Fig. 4 (c) breaks down the violation cost, showing that M3-FSM reduces the violation of SOC limitation by 88 % compared to M3-BR.

Fig. 5 (a) shows that, when imprecise load prediction is introduced, the comparisons of overall costs by using the three proposed methods (i.e., M1-BR-MPC, M3-BR, and M3-FSM) maintain almost the same as the ideal load prediction situation. However, the load deviations result in a small augmentation in overall operation cost for all three proposed methods. In contrast to the proposed methods, NoLL-MPC leads to a much higher overall violation cost, causing the highest total cost. According to Fig. 5 (a), the imprecise load prediction results in the overall operation cost increased by 0.83 %, 0.57 %, and 3.58 % when adopting M3-BR, M3-FSM, and M1-BR-MPC, respectively. This means that M1-BR-MPC is impacted more by the imprecise load prediction than M3-BR and M3-FSM, although it still performs the best among all methods. In addition, compared to M3-BR and M3-FSM, NoLL-MPC results in 6.6 and 152.81 times higher the overall violation cost.

Fig. 5 (b) breaks down the operation cost, showing similar comparison results of the three proposed methods for each index compared to Fig. 4 (a). In particular, M1-BR-MPC performs the best in terms of power loss and the second in terms of battery power changes among the three methods. NoLL-MPC performs similarly to M1-BR-MPC in terms of each breakdown operation cost. Fig. 5 (c) breaks down the violation cost, showing that the highest violation cost is the battery power violations caused by NoLL-MPC because of the load deviations. In contrast, when adopting the LL controller, the real-time load deviations result in neglectable impacts on each violation cost compared to Fig. 4 (a). According to Fig. 5 (a), NoLL-MPC causes high battery power violation costs. This results in the overall violation cost of NoLL-MPC being 6.6 and 152.81 times higher than that when adopting M3-BR and M3-FSM.

5.1.1. Simulation results of SOC and battery power

Fig. 6 and Fig. 7 demonstrate the SOC and the charging/discharging power of the four batteries on the LV buses for Case 1 when the maximum ± 5 % load deviations are introduced. The M3-BR and M3-FSM methods keep the battery charging to increase the SOC to the upper bound (0.9), whatever the initial values of SOC are. In addition, Fig. 7 (c) and (d) show that M3-FSM stops batteries charging after the SOC exceeds the target upper bound to avoid overcharging, while M3-

BR keeps batteries switching between charging and discharging, resulting in potential harmful impacts to battery health and SOC fluctuating around the upper bound. In contrast to M3-BR and M3-FSM, Fig. 6 shows that M1-BR-MPC charges a battery for a longer time when its SOC initial value is closer to the lower bound (0.3). However, when the SOC initial value is close to the upper bound, M1-BR-MPC tends to maintain the SOC without charging or discharge to avoid additional power losses, unnecessary switching between charging and discharging, and SOC boundary violations. Compared to M3-BR and M3-FSM, M1-BR-MPC reduces the cost of power losses by 13.71 % and 11.54 %, respectively, according to Fig. 5 (b). In addition, compared to M3-BR, M3-FSM and M1-BR-MPC reduce the battery power changes by 66.68 % and 10.42 %, respectively.

Fig. 6 and Fig. 7 also show that NoLL-MPC results in a similar change tendency of SOC and battery power compared to M1-BR-MPC, because both methods refer to decisions from the online MPC. However, without LL control, battery 1, 2 and 4 would exceed their maximum charging/discharging limitations (± 3 kW), such as the example in Fig. 7 (a).

5.1.2. Simulation results of generator output power

Fig. 8 illustrates the generator output power in the EPS for Case 1. The APU is not started in normal conditions using all control methods. In general, the output power of Generator 1 is more than that of Generator 2 in most flight stages using all control methods. Because when loads allocated on Generator 1 and 2 are almost the same, Generator 1 supplies more power to charge the batteries on LV bus 1 and 2, while the batteries on LV bus 3 and 4 require less power from Generator 2. In addition, NoLL-MPC provides results similar to those of M1-BR-MPC because the generators are assumed to be capable of supplying loads with predefined deviations.

5.1.3. Simulation results of cells' input power

Fig. 9 presents the cells' input power in the EPS for Case 1. According to the configuration results, each LV bus is supported by three cells; for example, LV bus 1 is supplied by Cells 1–3. The power allocated for Cells 1–3 is the same when adopting M3-BR and M3-FSM, because they apply rules to equivalently share the power among the cells connected to one LV bus. In contrast, when adopting M1-BR-MPC, Cell 3 is less used compared to Cell 1, because M1-BR-MPC allocates power to cells differently to reduce power losses. Similar comparisons and conclusions can be observed for the cells on other LV buses, which indicates that the EPS operates following the designed control strategies. In addition, NoLL-MPC shows a similar tendency to M1-BR-MPC. However, without the LL controller, the cells' power cannot be adjusted to prevent the battery power from exceeding the limits. For example, as illustrated in Fig. 7 (a) and Fig. 9, during 0 min - 2 min, M1-BR-MPC reduces the power allocated to Cell 1–3 compared to NoLL-MPC to avoid Battery 1 being overcharged, which verifies the effectiveness of the LL controller in the collaboration mode for responses of real-time load changes.

5.2. Case 2: EPS faulty scenario

This case aims to verify the controller's capability to respond to the component failures following the operational constraints and compare the performance in the fault condition. Several fault scenarios are assumed during different flight stages, including failure events for: Battery 4; Cell 10; Generator 1; the connection between HVB 2 and Cell 7 (S_{27}^{hvc}); and the connection between HVB 1 and Cell 1 (S_{11}^{ch}). The failures are assumed to occur at the specified time instances, and the components then remain faulty for the duration of the flight, as listed in Table 6.

Fig. 10 (a) shows that the faulty condition results in the overall operation and total costs rising for all proposed methods compared to the EPS normal condition. In terms of the overall violation cost, faulty conditions cause the cost to rise when using M4-BR and M4-FSM, while M2-BR-MPC can avoid violations even in the faulty scenario. Among all three methods, M2-BR-MPC achieves the minimum overall operation and violation costs among all methods studied. Compared Fig. 10 (a) to Fig. 4 (a), the faulty condition results in M3-BR and M3-FSM increasing the overall operation cost by 104 % and 90 %, respectively, and increasing the overall violation cost by 44 % and 869 %, respectively. In contrast, the faulty condition only results in M2-BR-MPC increasing the overall operation cost by 80 %. According to Fig. 10 (a), compared to M4-BR and M4-FSM, M2-BR-MPC reduces the overall operation cost is reduced by 20.93 % and 14.4 %, respectively, and the total cost by 25.64 % and 18.92 %, respectively. Compared to M4-BR, M4-FSM reduced the overall operation cost and total cost by 8.3 % for each.

Fig. 10 (b) breaks down the operation cost, showing that the load shedding and switching costs exceed the SOC cost in the EPS faulty scenario compared to Fig. 4 (b). The dominant operation costs in the EPS faulty scenarios are power losses, switching activities, and load shedding. Among all methods, M2-BR-MPC performs the best in all three dominant operation costs, while it causes the highest SOC cost compared to M4-BR and M4-FSM. In contrast, M4-FSM performs the best in reducing the battery power changes, while M4-BR performs best in maintaining SOC. Fig. 10 (c) breaks down the violation cost, showing that M4-BR and M4-FSM cause SOC violations, while M4-FSM reduces the violation of SOC limitation by 18.79 % compared to M4-BR.

5.2.1. Simulation results of SOC and battery power

Fig. 11 and Fig. 12 demonstrate the SOC and the charging/discharging power of four batteries on the LV buses for Case 2. Fig. 13 presents the connection of LV buses. The SOC and battery charging/discharging power are impacted by how the EPS is configured to cope with power shortage when adopting the proposed methods.

Firstly, Battery 2 in Fig. 11 (b) is not impacted by the failures; therefore, all methods maintain similar decisions for Battery 2 compared to Case 1 Fig. 6 (b). Secondly, at 1000s (16.17 min), Battery 4 is out of service and disconnected. Hence, all methods keep the power of Battery 4 at 0 kW in the following flight stages in Fig. 12 (d), and its SOC remains unchanged in Fig. 11 (d). Thirdly, Fig. 11 (a) shows that all methods keep Battery 1 charging initially because the initial SOC is close to the lower bound. However, at 1000s (16.17 min), M2-BR-MPC, M4-BR, and M4-FSM connects LVB 1 with LVB 4 following rules in the LL controller. Battery 1 is then discharged after 50 min, because the disconnection of Cell 10 results in insufficient power to LVB 4, and LVB 4 is supplied by Battery 1 with the connection of LVB 1 and LVB 4. This discharging tendency is changed at different moments when different methods are adopted.

M2-BR-MPC maintains the connection decisions of M2 in the LL until 85 min, to avoid the switching activities. After 85 min, LVB 3 is connected to LVB 4 by M2-BR-MPC to supply the loads on both buses and stop the discharge of Battery 1, avoiding the SOC violating the lower bound (0.3). Fig. 11 (c) shows that Battery 3 is discharged to supplied LVB 3 and 4 during 85–110 min. In contrast, without the online MPC considering future status, M4-BR and M4-FSM cause the SOC of Battery 1 to drop below the lower bound, and cause load shedding on LVB 1 and 4 during 98–110 min in Fig. 16 (c) and (l). As presented in Fig. 11, M4-FSM keeps load shedding during the 98–110 min to maintain the charge of Battery 1, while M4-BR alternates between charging the battery and reconnecting loads. The discussions above indicate that M2-BR-MPC achieves a better balance among managing battery SOC, load

shedding, and switching activities than M4-BR and M4-FSM.

5.2.2. Simulation results of generator output power

Fig. 14 illustrates the generator/APU output power for Case 2. Fig. 14 (a) shows that the generator is disconnected because of the failure at 3000 s (50 min). The APU is started by the LL controller in all proposed methods, and is connected to the HV bus 1 (HVB 1) to replace Generator 1 after 20 s for starting up in Fig. 14 (c). During the APU starting period (50 min to 50.33 min), Generator 2 is connected to HVB 1 to supply the EPS, and mid (Load 3) and low (Load 4) priority HV/LV loads are shed by all methods, as presented in Fig. 11 and Fig. 12.

5.2.3. Simulation results of cells' input power

The input power of each cell is presented in Fig. 15. Fig. 15 (j) shows that failure occurs in Cell 10 at 2000s (33.33 min), which is disconnected by the LL controller in all methods. Therefore, the output power of Cell 10 is 0 kW afterwards. In addition, all cells' power drops at 50 min when Generator 1 fails, but the power is recovered once the APU is connected. Fig. 15 (g) and (a) show that the power drops at 4000 s (66.67 min) and 5000 s (83.33 min) for Cell 7 and Cell 1, respectively, because of the connection failure. However, the LL controller switches their connection with Cell 6 and Cell 12 in all methods. Because the online MPC avoids transmission switching, the connection remains unchanged by all methods. In addition, similar to Case 1, Fig. 15 shows that M2-BR-MPC provides optimal power allocation among converters compared to M4-BR and M4-FSM. This is one of the reasons that M2-BR-MPC reduced more power losses compared to M4-BR and M4-FSM, by 21 % and 14 %, respectively.

5.2.4. Simulation results of load shedding and switching

Fig. 16 and Fig. 17 present the states of the non-critical load connections on LV and HV buses, respectively. HV/LV mid and low priority loads (i.e., Load 3 and Load 4 on each bus) are shed after Generator 1 fails (50 min) and during the APU starting time (50 min to 50.33 min) by all methods. After the APU is connected to HVB 1, loads are connected back. Then, M2-BR-MPC controls the EPS without future load shedding, while low-priority loads (Load 4) are shed on LVB 1 and LVB 4 during the 98–110 min by the M4-BR and M4-FSM. M2-BR-MPC performs the best in reducing load shedding among all methods. As presented in Fig. 10 (b), compared to M4-BR and M4-FSM, M2-BR-MPC reduces the load shedding by 66.49 % and 74.85 %, respectively. Compared to M4-BR, the load shedding increases by 33.25 % when M4-FSM is adopted.

In addition to load shedding, the count of switching activities is listed for all methods in Table 7. Compared to M4-BR and M4-FSM, M2-BR-MPC increases the switching of the transmission links by 15.38 %, which is caused by the change of LV bus interconnections. However, load switching is reduced by 45.45 % and 14.29 % compared to the other two methods when M2-BR-MPC is adopted. In addition, M4-FSM reduces the load switching activities by 36.36 % compared to M4-BR.

The above discussions indicate that M2-BR-MPC performs the best in reducing load shedding and switching activities by collaboration between the two levels of EMS. The independent LL controller can still make decisions for configurations and load shedding to meet operational constraints, while M4-FSM performs better than M4-BR in avoiding continuous load switching, although this can increase load shedding.

5.3. Summary of the case studies

In summary, when the EMS runs in the collaborative mode, with both HL and LL controllers (i.e., M1-BR-MPC and M2-BR-MPC), it achieves the best control performance in reducing both operation and violation

costs in all cases. This is because the online MPC in HL control provides optimal decisions in minimising operation costs in both normal and faulty scenarios, although introducing limited load deviations to the prediction values can slightly impair the performance. In addition, the LL controller is reliable in responding to quick load changes and failure occurrences to avoid violations. In contrast, when the online MPC is unavailable, the EMS runs in independent modes (i.e., M3-BR, M3-FSM, M4-BR, and M4-FSM), and violations are effectively controlled regardless of load deviations and faulty conditions. Although the independent modes cannot achieve the best operation costs, the EMS performance can be improved by improving the rules, such as adopting FSM rather than BR.

6. Conclusions

In this research, a two-level hierarchical EMS was designed to supervise the entire EPS operation in different time scales and operational scenarios. The HL controller was based on the optimisation scheme of MILP-MPC to improve the long-term EPS performance using future predictions. To provide quick responses to short-term system changes, such as changing load demands and/or failures, a rule-based LL controller with a faster clock was proposed. The LL contains four modes, allowing it to either cooperate with a HL online MPC or operate independently, in either EPS normal or faulty conditions. Moreover, two methods, BR and FSM, were applied in the rule design for the LL independent modes. Two cases were simulated to verify the effectiveness of the proposed hierarchical control. In addition, the performance of the hierarchical control in different modes was evaluated and compared.

It was shown that the HL controller on its own was incapable of reacting fast enough to EPS changes (e.g., loads changing or failures occurring), whereas the LL controller on its own (independent) was less effective at optimising the cost. The best results are obtained when both controllers work together, dealing effectively with both load power deviations and component failures. In addition, regardless of the availability of the HL controller, the LL controller was always able to maintain the EPS safe operation in all scenarios.

For safety reasons, conventional EMS for aircraft EPSs often completely rely on predefined rules to ensure all control strategies are deterministic, and reliable, however, this makes it challenging to improve EPS performance. This study provides researchers with an innovative controller design methodology which ensures that strict safety requirements are guaranteed (by the predictability of the predefined rules LL deterministic rules), while allowing the HL controller to be flexible enough to provide various efficiency optimisation strategies. This study should inspire further work on multi-level optimisation, having shown the benefits of the coordination, where the LL controller ensures that the hard (safety) constraints are satisfied, while the HL controller can adopt a variety of deterministic or nondeterministic techniques to achieve the optimisation/preferred targets.

CRedit authorship contribution statement

Xin Wang: Writing – review & editing, Writing – original draft, Visualization, Validation, Software, Methodology, Investigation, Formal analysis, Data curation, Conceptualization. **Jason Atkin:** Writing – review & editing, Supervision, Resources, Project administration, Conceptualization. **Serhiy Bozhko:** Writing – review & editing, Supervision, Resources, Project administration, Funding acquisition.

Declaration of competing interest

The authors declare that they have no known competing financial interests or personal relationships that could have appeared to influence the work reported in this paper.

Acknowledgements

This work has been funded by H2020 Cleansky-2 JTI (REG) under grant agreement number 785416.

Data availability

Data will be made available on request.

References

- [1] Federal Aviation Administration. Aviation emissions, impacts & mitigation. 2015.
- [2] Federal Aviation Administration. FY2024–2044 FAA aerospace fore cast. 2024.
- [3] Collins JM, McLarty D. All-electric commercial aviation with solid oxide fuel cell-gas turbine-battery hybrids. *Appl Energy* 2020;265:114787. <https://doi.org/10.1016/j.apenergy.2020.114787>. vol.
- [4] Federal Aviation Administration. Aviation climate action plan. 2021.
- [5] Airbus Operations Sas. More open electrical technologies. 2006. <https://cordis.europa.eu/project/id/30861/fr>.
- [6] Federal Aviation Administration. Clean Aviation Joint Undertaking. 2021. https://european-union.europa.eu/institutions-law-budget/institutions-and-bodies/search-all-eu-institutions-and-bodies/clean-aviation-joint-undertaking_en.
- [7] Wileman AJ, Aslam S, Perinpanayagam S. A road map for reliable power electronics for more electric aircraft progress in aerospace sciences a road map for reliable power electronics for more electric aircraft. *Prog Aerosp Sci* 2021:100739. <https://doi.org/10.1016/j.paerosci.2021.100739>. no. October, p.
- [8] Airbus. Environment matters for the future of aerospace. *Airbus Environ* 2019: 1–26.
- [9] McKinsey&Company. Decarbonizing aviation: executing on net-zero goals. 2023. <https://www.mckinsey.com/industries/aerospace-and-defense/our-insights/decarbonizing-aviation-executing-on-net-zero-goals/>.
- [10] Ollas P, et al. Evaluating the role of solar photovoltaic and battery storage in supporting electric aviation and vehicle infrastructure at visby airport. *Appl Energy* 2023;352:121946. <https://doi.org/10.1016/j.apenergy.2023.121946>. vol.
- [11] Sarlioglu B, Morris CT. More electric aircraft: review, challenges, and opportunities for commercial transport aircraft. *IEEE Trans Transp Electrif* 2015;1(1):54–64. <https://doi.org/10.1109/TTE.2015.2426499>. vol.
- [12] Wheeler P, Bozhko S. The more electric aircraft. *IEEE Electr Mag* 2014;1–7. no. December.
- [13] Wang X, Atkin J, Hill C, Bozhko S. Power allocation and generator sizing optimisation of more-electric aircraft on-board electrical power during different flight stages. AIAA Propuls Energy Forum Expo 2019;2019:1–10. <https://doi.org/10.2514/6.2019-4485>. no. August.
- [14] Liang S, He LK, Wu Y, Zhao H, Li H, Li W. Overview and analysis of electric power systems for more/all electric aircraft. *IECON Proc Industrial Electron Conf* 2023. <https://doi.org/10.1109/IECON51785.2023.10312392>. no. c.
- [15] Barzkar A, Ghassemi M. Components of electrical power systems in more and all-electric aircraft: a review. *IEEE Trans Transp Electrif* 2022;8(4):4037–53. <https://doi.org/10.1109/TTE.2022.3174362>. vol.
- [16] Guerrero JM, Chandorkar M, Lee TL, Loh PC. Advanced control architectures for intelligent microgrids part I: decentralized and hierarchical control. *IEEE Trans Ind Electron* 2013;60(4):1254–62. <https://doi.org/10.1109/TIE.2012.2194969>. vol.
- [17] Ma T, Li M, Xu H, Jiang R, Ni J. Study on multi-time scale frequency hierarchical control method and dynamic response characteristics of the generation-grid-load-storage type integrated system under double-side randomization conditions. *Appl Energy* 2024:123436. <https://doi.org/10.1016/j.apenergy.2024.123436>. vol. 367, no. April.
- [18] Giraud X, Piquet H, Budinger M, Roboam X, Sartor M, Vial S. Knowledge-based system for aircraft electrical power system reconfiguration. *Electr Syst Aircraft Railw Sh Propulsion ESARS* 2012;2048:1–6. <https://doi.org/10.1109/ESARS.2012.6387377>. vol.
- [19] Zhu J, Xiong X, Zhang J, Shen G, Xu Q, Xue Y. A rule based comprehensive approach for reconfiguration of electrical distribution network. *Electr Power Syst Res* 2009;79(2):311–5. <https://doi.org/10.1016/j.epsr.2008.07.001>. vol. no.
- [20] Farrokhi E, Safari P, Ghoreishy H. A rule-based energy management strategy with current estimation for controlling grid connected hybrid energy storage System. 14th Power Electron Drive Syst Technol Conf PEDSTC 2023:1–7. 2023, no. Pedstc. 2023. <https://doi.org/10.1109/PEDSTC57673.2023.10087163>.
- [21] Chakraborty S, Modi G, Singh B. A cost optimized-reliable-resilient-realtime-rule-based energy management scheme for a SPV-BES-based microgrid for smart building applications. *IEEE Trans Smart Grid* 2023;14(4):2572–81. <https://doi.org/10.1109/TSG.2022.3232283>. vol. no.
- [22] Mohamed MAA, Yeoh SS, Atkin JA, Hussaini H, Bozhko S. Efficiency focused energy management strategy based on optimal droop gain design for more electric aircraft. *IEEE Trans Transp Electrif* 2022;8(4):4205–18. <https://doi.org/10.1109/TTE.2022.3159731>. vol.
- [23] Wang Y, Sun Z, Chen Z. Energy management strategy for battery/supercapacitor/fuel cell hybrid source vehicles based on finite state machine. *Appl Energy* 2019: 113707. <https://doi.org/10.1016/j.apenergy.2019.113707>. vol. 254, no. August.
- [24] Phan Van L, Hoang Hieu L, do Chi K, Takano H, Nguyen Duc T. An improved state machine-based energy management strategy for renewable energy microgrid with hydrogen storage system. *Energy Rep* 2023;9:194–201. <https://doi.org/10.1016/j.egy.2022.10.385>. vol.

- [25] Fu X, Wang B, Yang J, Liu S, et al. A rule-based energy management strategy for a light-duty commercial P2 hybrid electric vehicle optimized by dynamic programming. SAE Tech Pap 2021. <https://doi.org/10.4271/2021-01-0722>.
- [26] Jamal S, Pasupuleti J, Ekanayake J. A rule-based energy management system for hybrid renewable energy sources with battery bank optimized by genetic algorithm optimization. Sci Rep 2024;14(1):1–17. <https://doi.org/10.1038/s41598-024-54333-0>. vol.
- [27] Xu L, et al. A comprehensive review on fuel cell uav key technologies : propulsion system, management strategy, and design procedure. IEEE Trans Transp Electr 2022;8(4):4118–39. <https://doi.org/10.1109/TTE.2022.3195272>. vol.
- [28] Ma R, Chai X, Geng R, Xu L, Xie R, Zhou Y. Recent progress and challenges of multi-stack fuel cell systems : Fault detection and reconfiguration, energy management strategies, and applications. vol285; March, 2023. <https://doi.org/10.1016/j.enconman.2023.117015>. no.
- [29] Hossain Lipu MS, et al. A review of controllers and optimizations based scheduling operation for battery energy storage system towards decarbonization in microgrid: challenges and future directions. J Clean Prod 2022;132188. <https://doi.org/10.1016/j.jclepro.2022.132188>. vol. 360, no. April.
- [30] Li S, et al. Hybrid power system topology and energy management scheme design for hydrogen-powered aircraft. IEEE Trans Smart Grid 2024;15(2):1201–12. <https://doi.org/10.1109/TSG.2023.3292088>. vol. no.
- [31] Gangwar T, Padhy NP, Jena P. Energy management approach to battery energy storage in unbalanced distribution networks. IEEE Trans Ind Appl 2024;60(1):1345–56. <https://doi.org/10.1109/TIA.2023.3321030>. vol. no.
- [32] Zou Y, Xu Y, Zhang C. A risk-averse adaptive stochastic optimization method for Transactive energy management of a multi-energy microgrid. IEEE Trans Sustain Energy 2023;14(3):1599–611. <https://doi.org/10.1109/TSTE.2023.3240184>. vol.
- [33] Zhang Y, Yu Y, Su R, Chen J. Power scheduling in more electric aircraft based on an optimal adaptive control strategy. IEEE Trans Ind Electron 2019. <https://doi.org/10.1109/tie.2019.2960718>. vol. PP, no. December. pp. 1–1, 2019.
- [34] Zhang J, Roumeliotis I, Zolotas A. Model-based fully coupled propulsion-aerodynamics optimization for hybrid electric aircraft energy management strategy. Energy 2022;245:123239. <https://doi.org/10.1016/j.energy.2022.123239>. vol.
- [35] Gao P, Li Y, Yao W, Zheng X, Zhang C. Optimization of hybrid energy storage system sizing with considering energy management strategy for high-power pulsed load in aircraft. IEEE Trans Veh Technol 2023;72(4):4525–37. <https://doi.org/10.1109/TVT.2022.3228734>. vol.
- [36] Zheng F, Chen Y, Zhang J, Cheng F, Zhang J. A two-stage energy management for integrated thermal/energy optimization of aircraft airborne system based on Stackelberg game. Energy 2023;269:126506. <https://doi.org/10.1016/j.energy.2022.126506>. volno. December 2022.
- [37] Shi W, Huangfu Y, Xu L, Pang S. Online energy management strategy considering fuel cell fault for multi-stack fuel cell hybrid vehicle based on multi-agent reinforcement learning. Appl Energy 2022;120234. <https://doi.org/10.1016/j.apenergy.2022.120234>. vol. 328, no. November.
- [38] He L, Chen F, Tian P, Gou H. An improved energy management strategy for hybrid electric powered aircraft based on deep reinforcement learning. Aerosp Sci Technol 2024;149:109137. <https://doi.org/10.1016/j.ast.2024.109137>. volno. December 2023.
- [39] Shan C, Sun K, Ji X, Cheng D. A reconfiguration method for photovoltaic array of stratospheric airship based on multilevel optimization algorithm. Appl Energy 2023;121881. <https://doi.org/10.1016/j.apenergy.2023.121881>. vol352, no. September.
- [40] Silveira CLB, Tabares A, Faria LT, Franco JF. Mathematical optimization versus metaheuristic techniques: a performance comparison for reconfiguration of distribution systems. Electr Power Syst Res 2021;196. <https://doi.org/10.1016/j.epsr.2021.107272>. vol. no. April.
- [41] Ghaemi Z, Tran TTD, Smith AD. Comparing classical and metaheuristic methods to optimize multi-objective operation planning of district energy systems considering uncertainties. Appl Energy 2022;119400. <https://doi.org/10.1016/j.apenergy.2022.119400>. vol. 321, no. March.
- [42] Zong Y, Kullmann D, Thavlov A, Gehrke O, Bindner HW. Application of model predictive control for active load management in a distributed power system with high wind penetration. IEEE Trans Smart Grid 2012;3(2):1055–62. <https://doi.org/10.1109/TSG.2011.2177282>. vol.
- [43] Ordoñez JG, Barco-Jiménez J, Pantoja A, Revelo-Fuelagán J, Canelo-Becerra JE. Comprehensive analysis of MPC-based energy management strategies for isolated microgrids empowered by storage units and renewable energy sources. J Energy Storage 2024;112127. <https://doi.org/10.1016/j.est.2024.112127>. vol. 94, no. May.
- [44] Maasoumy M, Nuzzo P, Iandola F, Kamgarpour M, Sangiovanni-Vincentelli A, Tomlin CJ. Optimal load management system for aircraft electric power distribution. IEEE Conf Decis Control 2013:2939–45. <https://doi.org/10.1109/CDC.2013.6760330>.
- [45] Shahsavari B, Maasoumy M, Sangiovanni-Vincentelli A, Horowitz R. Stochastic model predictive control design for load management system of aircraft electrical power distribution. Am Control Conf 2015:3649–55. s, <https://doi.org/10.1109/ACC.2015.7171897>.
- [46] Zhang Y, Chen J, Yu Y. Distributed power management with adaptive scheduling horizons for more electric aircraft. Int J Electr Power Energy Syst 2021;106581. <https://doi.org/10.1016/j.ijepes.2020.106581>. vol. 126, no. PA.
- [47] Doff-Sotta M, Cannon M, Bacic M. Predictive energy management for hybrid electric aircraft propulsion systems. IEEE Trans Control Syst Technol 2023;31(2):602–14. <https://doi.org/10.1109/TCST.2022.3193295>. vol.
- [48] Zhang J, Roumeliotis I, Zolotas A. Nonlinear model predictive control-based optimal energy management for hybrid electric aircraft considering aerodynamics-propulsion coupling effects. IEEE Trans Transp Electr 2022;8(2):2640–53. <https://doi.org/10.1109/TTE.2021.3137260>. vol.
- [49] Ma R, Song J, Zhang Y, Zhang H, Yuan M. Lifetime-optimized energy management strategy for fuel cell unmanned aircraft vehicle hybrid power system. IEEE Trans Ind Electron 2023;70(9):9046–56. <https://doi.org/10.1109/TIE.2022.3206687>. vol.
- [50] Zhang Y, et al. An energy efficient power management solution for a fault-tolerant more electric engine/aircraft. IEEE Trans Ind Electron July 2019;66(7):5663–75. <https://doi.org/10.1109/TIE.2018.2877169>.
- [51] Wang X, Bazmohammadi N, Atkin J, Bozhko S, Guerrero JM. Chance-constrained model predictive control-based operation management of more-electric aircraft using energy storage systems under uncertainty. J Energy Storage 2022;55:105629. <https://doi.org/10.1016/j.est.2022.105629>. vol.
- [52] Prodan I, Zio E, Stoican F. Fault tolerant predictive control design for reliable microgrid energy management under uncertainties. Energy 2015;91:20–34. <https://doi.org/10.1016/j.energy.2015.08.009>. vol.
- [53] Marquez JJ, Zafra-Cabeza A, Bordons C, Ridao MA. A fault detection and reconfiguration approach for MPC-based energy management in an experimental microgrid. Control Eng Pract 2021;107:104695. <https://doi.org/10.1016/j.conengprac.2020.104695>. vol. no. August 2020.
- [54] Haubensak L, Strahl S, Braun J, Faulwasser T. Towards real-time capable optimal control for fuel cell vehicles using hierarchical economic MPC. Appl Energy 2024;123223. <https://doi.org/10.1016/j.apenergy.2024.123223>. vol. 366, no. March.
- [55] Zhang H, Saudemont C, Robyns B, Meuret R. Comparison of different DC voltage supervision strategies in a local power distribution system of more electric aircraft. Math Comput Simul 2010;81(2):263–76. <https://doi.org/10.1016/j.matcom.2010.05.009>. vol.
- [56] Zhang H, Mollet F, Saudemont C, Robyns B. Experimental validation of energy storage system management strategies for a local DC distribution system of more electric aircraft. IEEE Trans Ind Electron 2010;57(12):3905–16. <https://doi.org/10.1109/TIE.2010.2046575>. vol.
- [57] Jiang Z, Raziei SA. Hierarchical model predictive control for real-time energy-optimized operation of aerospace systems. AIAA Propuls Energy Forum Expo 2019; 2019:1–16. <https://doi.org/10.2514/6.2019-4487>. no. August.
- [58] Koeln JP, Pangborn HC, Williams MA, Kawamura ML, Alleyne AG. Hierarchical control of aircraft electro-thermal systems. IEEE Trans Control Syst Technol 2020; 28(4):1218–32. <https://doi.org/10.1109/TCST.2019.2905221>. vol.
- [59] Akstrand CT, Tannous PJ, Wagenmaker MJ, Pangborn HC, Alleyne AG. Hierarchical predictive control of an unmanned aerial vehicle integrated power, propulsion, and thermal management system. IEEE Trans Control Syst Technol 2023;31(3):1280–95. <https://doi.org/10.1109/TCST.2022.3220913>. vol. no.
- [60] Wu Y, et al. Integrated battery thermal and energy management for electric vehicles with hybrid energy storage system: a hierarchical approach. Energy Convers Manag 2024;317:118853. <https://doi.org/10.1016/j.enconman.2024.118853>. vol. no. July.
- [61] Liu H, Fan A, Li Y, Bucknall R, Chen L. Hierarchical distributed MPC method for hybrid energy management: a case study of ship with variable operating conditions. Renew Sust Energ Rev 2024;189:113894. <https://doi.org/10.1016/j.rser.2023.113894>. vol. no. PA.
- [62] Kaysal A, Koroğlu S, Oğuz Y. Hierarchical energy management system with multiple operation modes for hybrid DC microgrid. Int J Electr Power Energy Syst 2021;141:2022. <https://doi.org/10.1016/j.ijepes.2022.108149>. vol. no. November.
- [63] Elkazaz M, Sumner M, Naghiyev E, Pholboon S, Davies R, Thomas D. A hierarchical two-stage energy management for a home microgrid using model predictive and real-time controllers. Appl Energy 2020;269:115118. <https://doi.org/10.1016/j.apenergy.2020.115118>. vol. no. April.
- [64] Restrepo M, Cañizares CA, Simpson-porcio JW, Su P, Taruc J. Optimization- and rule-based energy management systems at the canadian renewable energy laboratory microgrid facility. Appl Energy 2021;290:116760. <https://doi.org/10.1016/j.apenergy.2021.116760>. vol. no. October 2020.
- [65] Nagpal H, Avramidis II, Capitanescu F, Madureira AG. Local energy communities in service of sustainability and grid flexibility provision: hierarchical management of shared energy storage. IEEE Trans Sustain Energy 2022;13(3):1523–35. <https://doi.org/10.1109/TSTE.2022.3157193>. vol.
- [66] Hong YY, Alano FI. Hierarchical energy management in islanded networked microgrids. IEEE Access 2022;10:8121–32. <https://doi.org/10.1109/ACCESS.2022.3143307>. vol.
- [67] Yang Y, Yang Y, Xie C, Xu L, Liu Y, Shi H. A hierarchical energy management strategy for DC microgrid hybrid energy storage systems based on fractional-order sliding mode controller. J Energy Storage 2024;99:113307. <https://doi.org/10.1016/j.est.2024.113307>. vol. no. PB.
- [68] Ge Y, Song B, Pei Y, Mollet Y, Gyselinck J. A fuzzy logic based method for fault tolerant hierarchical load management of more electric aircraft. Proc Inst Mech Eng Part G J Aerosp Eng Nov. 2018;233(10):3846–56. <https://doi.org/10.1177/0954410018807598>. vol. no.
- [69] Wheeler P, Bozhko S. The more electric aircraft: technology and challenges. IEEE Electr Mag 2014;2(4):6–12. <https://doi.org/10.1109/MELE.2014.2360720>. vol. no.
- [70] Buticchi G, Bozhko S, Liserre M, Wheeler P, Al-Haddad K. On-board microgrids for the more electric aircraft—technology review. IEEE Trans Ind Electron 2019;66(7):5588–99. <https://doi.org/10.1109/TIE.2018.2881951>. vol. no.
- [71] Wang X, Atkin J, Yeoh S, Bozhko S. Optimised architecture design for an MEA power distribution system considering load profile and fault-tolerance. In: IEEE

- international conference on electrical systems for aircraft, railway, ship propulsion and road vehicles & international transportation electrification conference (ESARS-ITEC); 2023. p. 1–7. <https://doi.org/10.1109/ESARS-ITEC57127.2023.10114839>. 2023.
- [72] Wang X, Atkin J, Bazmohammadi N, Bozhko S, Guerrero JM. Optimal load and energy management of aircraft microgrids using multi-objective model predictive control. *Sustainability* 2021;13(24). <https://doi.org/10.3390/su132413907>. vol. no.
- [73] Wang X, Atkin J, Bozhko S, Hill C. Application of a MILP-based algorithm for power flow optimisation within more-electric aircraft electrical power systems. 21st Eur Conf Power Electron Appl 2019. <https://doi.org/10.23919/EPE.2019.8915388>. *EPE 2019 ECCE Eur.*, p. P.1-P.8, 2019.
- [74] Wang H, Alattas KA, Mohammadzadeh A, Sabzalian MH, Aly AA, Mosavi A. Comprehensive review of load forecasting with emphasis on intelligent computing approaches. *Energy Rep* 2022;8:13189–98. <https://doi.org/10.1016/j.egy.2022.10.016>. vol.
- [75] Todd R, Bryan F, Forsyth AJ, Gan C, Bossard J. Effects of electrical power off-take on finite inertia mechanical systems. *IEEE Energy Convers Congr Expo Energy Convers Innov A Clean Energy Futur ECCE 2011*:1476–82. Proc., no. May 2015. 2011, <https://doi.org/10.1109/ECCE.2011.6063955>.
- [76] Seresinhe R, Lawson C. Electrical load-sizing methodology to aid conceptual and preliminary design of large commercial aircraft. *Proc Inst Mech Eng Part G J Aerosp Eng* 2015;229(3):445–66. <https://doi.org/10.1177/0954410014534638>. vol. no.
- [77] Xia X. *Dynamic power distribution management for all electric aircraft*. 2011 [Online]. Available: <https://core.ac.uk/download/pdf/140642.pdf>.
- [78] Wang X, Gao Y, Atkin J, Bozhko S. Neural network based weighting factor selection of mpc for optimal battery and load management in MEA. In: 23rd international conference on electrical machines and systems (ICEMS); 2020. p. 1763–8. <https://doi.org/10.23919/ICEMS50442.2020.9290968>. 2020.